



Catarina Martins Rodrigues

Licenciada em Engenharia de Micro e Nanotecnologia

Spray Coating of Oxide and Chalcogenide Semiconductor Layers for TFT Application

Dissertação para obtenção do Grau de Mestre em
Engenharia de Micro e Nanotecnologia

Orientador: Doutor Albert van Breemen, Investigador, Holst Centre
Co-orientador: Doutor Pedro Miguel Cândido Barquinha, Prof. Auxiliar,
FCT/UNL

Júri:

Presidente: Doutora Rodrigo Ferrão de Paiva Martins, Prof. Catedrático
Arguente: Doutora Rita Maria Mourão Salazar Branquinho, Prof. Auxiliar Convidada
Vogal: Doutor Pedro Miguel Cândido Barquinha, Prof. Auxiliar



FACULDADE DE
CIÊNCIAS E TECNOLOGIA
UNIVERSIDADE NOVA DE LISBOA

Outubro 2015

Spray Coating of Oxide and Chalcogenide Semiconductor Layers for TFT Application

© Catarina Martins Rodrigues

Faculdade de Ciências e Tecnologia

Universidade Nova de Lisboa

Spray Coating of Oxide and Chalcogenide Semiconductor Layers for TFT Applications

Copyright © Catarina Martins Rodrigues, Faculdade de Ciências e Tecnologia, Universidade Nova de Lisboa.

A Faculdade de Ciências e Tecnologia e a Universidade Nova de Lisboa têm o direito, perpétuo e sem limites geográficos, de arquivar e publicar esta dissertação através de exemplares impressos reproduzidos em papel ou de forma digital, ou por qualquer outro meio conhecido ou que venha a ser inventado, e de a divulgar através de repositórios científicos e de admitir a sua cópia e distribuição com objetivos educacionais ou de investigação, não comerciais, desde que seja dado crédito ao autor e editor.

ACKNOWLEDGEMENTS

After six months in the Netherlands, I have lost track of everyone that helped me throughout this journey. During this time aboard, I met and worked with incredible talented people, some of which I can call friends. The reported work would not be possible without the guidance and support of a large number of people. From these I would like to highlight and sincerely thank:

To Dr. Albert van Breemen, who supervise my day to day activities of my internship at the Holst Centre. For the guidance, time and patience you had, and for supporting me even when the experiments were not working as we expected. I simply can't thank you enough.

To Prof. Pedro Barquinha, who contacted Holst Centre to explore the possibility of my research internship there. Thank you so much for giving me the right advise, even when the thought of doing my master thesis project in another country seemed frightening and overwhelming. Your support and guidance in the beginning, as well as throughout my time in Eindhoven and especially in the final weeks is invaluable to me.

To Dr. Ashutosh Tripathi and Dr. Esger Smits for all the technical support and ideas shared in the meetings. To Dr. Gerwin Gelick, the head of our group at Holst Centre, for challenging me to think bigger. To Dr. Brian Coob for welcoming me to the group on my first day and showing me around.

To Wilco Keur from Philips, for helping me in first few weeks in the laboratory, and to everyone from Philips Research who shared with me a kind greeting every morning.

To TNO and the Holst Centre for supporting my project and allowing me to use their facilities.

To the group of interns from Holst Centre, with whom I shared my lunch breaks, but especially to Kevin Felter, for helping me in the laboratory and for discussing the problems I had during my research. Also, a special thanks to Daphné Lafond, for the amazing times we shared and for keeping me company during the busiest times. Despite the few months I had for that, I really enjoyed to meet you both.

To my colleagues and friends from FCT/UNL, for accompanying me through this past five years, for helping me grown as a person and as a professional, for your support and patience. I'm especially grateful to Ricardo Ramos and Daniel Pereira, for being such good listeners and friends.

To João Serafim, for your guidance, patience, care, friendship and love, thank you for your invaluable advice (yes, I did listen to some of it).

To my brother and sister, for always welcoming me home with a hug.

Last but not least, I dedicate this work to my parents. Thank you for your support, for believing in me and especially for being such good role models.

ABSTRACT

This work documents the deposition and optimization of semiconductor thin films using chemical spray coating technique (CSC) for application on thin-film transistors (TFTs), with a low-cost, simple method. CSC setup was implemented and explored for industrial application, within Holst Centre, an R&D center in the Netherlands. As zinc oxide had already been studied within the organization, it was used as a standard material in the initial experiments, obtaining typical mobility values of $0.14 \text{ cm}^2/(\text{V}\cdot\text{s})$ for unpatterned TFTs. Then, oxide X layer characteristics were compared for films deposited with CSC at 40°C and spin-coating. The mobility of the spin-coated TFTs was $10^3 \text{ cm}^2/(\text{V}\cdot\text{s})$ higher, presumably due to the lack of uniformity of spray-coated film at such low temperatures. Lastly, tin sulfide, a relatively unexplored material, was deposited by CSC in order to obtain functional TFTs and explore the device's potential for working as a phototransistor. Despite the low mobilities of the devices, a sensitive photodetector was made, showing drain current variation of nearly one order of magnitude under yellow light. CSC technique's simplicity and versatility was confirmed, as three different semiconductors were successfully implemented into functional devices.

Keywords: spray-coating, Thin-Film Transistors, zinc oxide, tin sulfide, phototransistor, spin-coating.

Resumo

Este trabalho documenta a deposição e otimização de filmes finos semicondutores utilizando a técnica química de *spray-coating* (CSC), para aplicação em transístores de filme fino (TFTs), com um método simples de baixo custo. O sistema de CSC foi implementado e explorado para aplicação industrial, no Holst Centre, um centro de I&D na Holanda. Como o óxido de zinco tinha já sido estudado dentro da organização, foi utilizado como material padrão nas experiências iniciais, obtendo valores de mobilidade típicos para TFTs não-padronizados de $0,14 \text{ cm}^2/(\text{V.s})$. Seguidamente, as características da camada de óxido X foram comparadas para filmes depositados por CSC a 40°C e por *spin-coating*. A mobilidade dos TFTs produzidos usando *spin-coating* foi $10^3 \text{ cm}^2/(\text{V.s})$ mais elevada, presumivelmente devido à irregularidade do filme produzido por *spray-coating* a temperaturas tão baixas. Finalmente, sulfeto de estanho (SnS), um material relativamente pouco explorado, foi depositado por CSC para obter TFTs funcionais e explorar o potencial do dispositivo para trabalhar como um fototransistor. Apesar das baixas mobilidades dos dispositivos, um fotodetector sensível foi fabricado, mostrando variações de corrente de dreno de quase uma ordem de grandeza sob luz amarela. Confirma-se a simplicidade e versatilidade da técnica de CSC, sendo implementados com sucesso três diferentes semicondutores em dispositivos funcionais.

Palavras-Chave: *spray-coating*, transístores de filme fino, óxido de zinco, sulfato de estanho, fototransístor, *spin-coating*.

LIST OF ABBREVIATIONS

CSC	Chemical Spray-Coating
EDS	Energy Dispersive x-ray Spectroscopy
FR	Solution Flow-Rate
IR	Infrared
LCD	Liquid Crystal Display
LED	Light Emitting Diode
MOSFET	Metal Oxide Semiconductor Field-Effect Transistor
PVD	Physical Vapor Deposition
R&D	Research and Development
SEM	Scanning Electron Microscope
SS	Subthreshold Swing
TFT	Thin-Film Transistor
TNO	<i>Netherlands Organization for Applied Scientific Research</i>
UV	Ultraviolet
RGB	Red, Green and Blue

LIST OF SYMBOLS

μ_{FE}	field-effect mobility ($m^2/(V.s)$)
μ_{SAT}	saturation mobility ($m^2/(V.s)$)
C_I	dielectric capacitance per unit area (F/m^2)
H	nozzle height or distance between nozzle and substrate (cm)
I_D	current between drain and source (A)
I_G	current between gate and source (A)
I_{OFF}	transistor off current (A)
I_{ON}	transistor on current (A)
L	channel length (μm)
t	deposition time (s)
T	substrate temperature during deposition ($^{\circ}C$)
V_D	voltage between drain and source (V)
V_G	voltage between gate and source (V)
V_{ON}	turn-on voltage (V)
V_T	threshold voltage (V)
W	channel width (μm)

TABLE OF CONTENTS

1.	Motivation and objectives.....	1
2.	Introduction.....	3
2.1.	Spray Coating: A Cost-Effective Thin Film Deposition Technique	3
2.1.1.	Spray Coating vs Spin Coating	4
2.2.	Oxide Semiconductor Materials for TFT application.....	5
2.3.	Chalcogenides as High Performance Switching Materials	5
2.3.1.	Tin Sulfide.....	5
2.4.	Thin-Film Transistor: A Brief Overview of Device Characteristics	6
2.4.1.	Phototransistor: A Device for Light Detection	7
3.	Materials and Methods	9
3.1.	Precursor Solutions	9
3.2.	Substrates.....	9
3.3.	Thin Film Deposition Methods	10
3.4.	Characterization Methods.....	10
4.	Results and Discussion	13
4.1.	Zinc Oxide Standard Experiment: Spray Coating System Optimization	13
4.1.1.	Zinc Oxide Thin Films.....	13
4.1.2.	Thin-Film Transistor Considerations.....	13
4.1.3.	Zinc Oxide Thin Film Transistors.....	14
4.2.	Oxide X Deposited by Spin-Coating and Spray-Coating	16
4.2.1.	Oxide X Thin Film Optimization	16
4.2.2.	Oxide X TFTs: performance comparison between the two techniques	17
4.3.	Case Study: SnS Thin-Films	21
4.3.1.	SnS Thin-Film Optimization	21
4.3.2.	TFTs electrical measurements	23
4.3.3.	Phototransistor.....	25
5.	Conclusions.....	29
6.	Future Perspectives.....	31
7.	Annexes	39

LIST OF FIGURES

Figure 2.1 – Schematic of a typical CSC setup, including possible components, adapted from [1].	4
Figure 2.2 - Characteristic curves of a TFT, with the output curves on the left and the transfer curves on the right. Adapted from [62] and [63].	7
Figure 3.1 – Schematic of the TFT devices structure. A) Transversal view. B) Top view of a ring transistor. The arrow represents the direction of current set for these devices throughout the entire project.	9
Figure 3.2 - Implemented CSC system. A) Setup placed inside the fume hood: Power supply for the mechanical rotation motor system (green), syringe pump (red), nozzle (yellow) and hot plate (blue). B) Temperature controller device.	10
Figure 4.1 - ZnO thin film characterization. A) Graph of thin film thickness (nm) dependence on deposition time (s), showing a linear relation. B) Profiles of three different films, with deposition times of 20, 40 and 60 s, showing the roughness of the layers.	13
Figure 4.2 - Schematic of the fringing electric field on unpatterned semiconductor layer of a typical TFT architecture. Adapted from [73].	14
Figure 4.3 – Electrical characterization of the ZnO TFTs. A) Transfer curves of ring transistors with three different channel thicknesses. Continuous and dashed lines represent drain and leakage currents, respectively. Arrows indicate the V_G sweep direction, showing a clockwise hysteresis. B) Output Curves of the ZnO TFT with film thickness of 15 nm.	15
Figure 4.4 – Optical images (on top) and film profiles (on the bottom) of oxide X samples deposited using different nozzle heights, of 5, 7,9 and 11 cm, for samples I1, I2, I3 and I4, respectively.	17
Figure 4.5 - Optical images of oxide X films deposited on transistor substrates. A) Using spray-coating with a fixed nozzle height of 11 cm. B) Using spin-coating.	18
Figure 4.6 - Electrical characterization of the Oxide X TFTs with L of 40, 20 and 10 μm . A) Transfer curves of spray-coated TFTs. B) Transfer curves of spin-coated TFTs. Arrows indicate the V_G sweep direction, showing a clockwise hysteresis.	18
Figure 4.7 – Optical images (on top) and film profiles (on the bottom) of SnS samples deposited using different nozzle heights, of 5, 7,9 and 11 cm, for samples I1, I2, I3 and I4, respectively.	22
Figure 4.8 - SEM images of the SnS films deposited at T of 300, 350 and 400 $^{\circ}\text{C}$.	23
Figure 4.9 – Comparison of the transfer curves of TFTs with SnS semiconductor layers deposited at different substrate temperatures (T). Arrows indicate the V_G sweep direction,	

showing a clockwise hysteresis.24

Figure 4.10 – Comparison of transfer curves of spray-coated SnS TFTs with different channel lengths located on the same substrate, with T at 350 °C. Arrows indicate the V_G sweep direction, showing a clockwise hysteresis.....25

Figure 4.11 - Transfer curves of SnS TFTs before, during and after exposure to a yellow light source. **A)** Transistor with channel length of 40 μm . **B)** Transistor with channel length of 10 μm . Arrows indicate the V_G sweep direction, showing a clockwise hysteresis in both TFTs..26

Figure 4.12 - Transient Response of a SnS phototransistor when exposed to light. **A)** Cycles of 20 seconds of light on and off. **B)** Analysis of a single cycle and consequent determination of fall and rise times.26

Figure 4.13 - Response of Spray-Coated TFTs to Infrared Light. **A)** Transfer curves of a TFT with $L=40 \mu\text{m}$ before, during and after IR light exposure. Arrows indicate the V_G sweep direction, showing a clockwise hysteresis. **B)** Transient response of the same TFT to IR light.27

LIST OF TABLES

Table 4.1 – Extrated characteristic parameter values from Figure 4.3 of the produced ZnO TFTs, considering different film deposition times (different thicknesses).15

Table 4.2 – Extrated characteristic parameters from Figure 4.6 of Oxide X TFTs when deposited by spin-coating and spray-coating, considering transistors with different channel lengths.19

Table 4.3 – Extracted characteristic parameters values from Figure 4.10 of the produced SnS TFTs, considering different transistor channel lengths.....25

LIST OF ANNEXES

Annex A - Prediction of the market demand for light sensors, where phototransistors can be incorporated, showing an increasing demand over the next few years.39

Annex B – Alignment mask used for the contacts of the transistor substrates, where the different transistor layouts can be seen.39

Annex C - Extraction method used for obtaining the characteristic parameters of the studied TFTs.....40

Annex D – Deposition parameters used for spray coating deposition of different samples of oxide X thin films and respective optical images and film profiles.41

Annex E – Optical images of solutions with different solvents: A – Water; B- Isopropanol and water in a 1:3 proportion; C – Isopropanol and water in a 3:1 proportion; D – Methanol.44

Annex F - Deposition parameters used in spray coating deposition of different samples of SnS thin-films and respective optical images.44

1. MOTIVATION AND OBJECTIVES

Although major research breakthroughs have been done in the past few years in the field of thin film deposition and its application to functional devices (such as thin-film transistors), most of physical vapor deposition (PVD) methods require the use of sophisticated and expensive instruments (namely vacuum pumps, electron beams or sputtering sources). Even though most PVD techniques present better film characteristics and, ultimately, better device performance, cheap chemical methods, such as the liquid phase chemical method spray coating (CSC), have been investigated for industrial applications and large scale deposition. These methods have attracted attention for their versatility (capability of achieving uniform layers of different materials) and throughput.

With this background in mind, this project was done for TNO and performed in the Holst Centre facilities, an independent R&D center located at the High Tech Campus Eindhoven, in the Netherlands. One of the goals of the organization is to provide functional, but simple solutions to industry, using as little resources as possible to achieve the projects' goals. For that reason, this work was done using inexpensive, but effective characterization and production tools, such as optical microscopy and profilometry, which supported the decisions made to move forward with the project.

Even though the CSC technique has been widely explored by many research groups and its broad versatility proved by the successful deposition of a wide range of thin films, this technique was relatively new at the Holst Centre. So, this project was focused on the deposition and optimization of thin films, with the objective of precisely controlling its final characteristics (thickness, roughness, etc.) by simply changing parameters of the system. The optimized films were then deposited on silicon substrates containing an insulator layer and electrodes, in order to obtain a transistor structure (from now on called transistor substrates). By testing the device functionality, an assessment of the films' quality could be made, in order to determine the technique's viability in industrial processes.

In the first tests, zinc oxide (ZnO) was used as a standard semiconductor material to confirm the system was working properly. This oxide was chosen due to the availability of studies in the literature and also because a Holst Centre group had already worked with it for TFT applications. Then, a commercial solution developed and provided by a company's partner was tested by request on the CSC system. The solution had been previously optimized for spin-coating technique, where a uniform oxide layer was deposited on a transistor structure and good, stable results were obtained. Since CSC is also a solution based deposition technique that requires less amount of material, the commercial solution was tested with this method and the results were compared to the spin-coated samples. For confidentiality reasons, the solution and material composition cannot be revealed. Therefore, the commercial solution and the material's layer will be presented as solution X and oxide X, respectively.

Lastly, a material that has not been explored for application in TFTs, tin sulfide (SnS), was studied as a semiconductor. This material has been previously researched for solar cell application, revealing high light absorption. So, the photodetection capabilities of the material were investigated by testing the produced TFTs to function as phototransistors.

Objectives

The project hereby described focus mainly on the CSC technique, as a cheap, scalable and easy to work with thin film deposition method. Functional thin-film transistors were produced and used as a proof of concept, showing that films with good properties can be deposited with the installed setup.

The main objective was to prove the technique's versatility by using it to successfully deposit thin films of different materials, as a way to determine the viability of implementing it in the industry. This goal was accomplished in three different ways that show a different perspective of the project:

- 1) Implementation and optimization of the initial setup, by depositing ZnO thin films as a standard experiment and using them as a semiconductor layer on a functional transistor.
- 2) Assessment of thin film quality of Oxide X by comparing the results of deposition by spin-coating (previously optimized) and spray-coating.

- 3) Case Study: Deposition of SnS layers aiming for the production of a functional device. The initial steps of an investigation of SnS to be used in a photodetecting device, such as a phototransistor, were performed.

Ultimately, the long term goal of the project would be to determine if the CSC technique could be used in industrial context, focusing on the formation of layers as thin (~10-50 nm) and uniform as possible.

2. INTRODUCTION

In this chapter, an introduction will be given on the relevant topics for the comprehension of the following chapters. As the developed work is based on the use of a simple, low-cost deposition technique, the CSC functionality will be described thoroughly. Then, previous studies on the semiconductor materials used will be presented, as well as a focus on the material deposited in the final case study, SnS. A direct, simple view of the functionality of a thin film transistor and its characteristic parameters will be presented. The chapter closes with a look into the final application proposed, the phototransistor.

Throughout the project, the CSC will be defined as a deposition method where a liquid precursor solution is vaporized into an aerosol, reaching a substrate (that could be heated or not) and creating a layer on it, as the precursors react. This designation covers both spray deposition at ambient temperature and spray pyrolysis, where usually the substrates must be heated up to, at least, 100°C [1].

2.1. Spray Coating: A Cost-Effective Thin Film Deposition Technique

When choosing the deposition technique to be used for the production of a thin film, there are a number of options, which are often divided in two groups: physical vapor deposition (PVD) and chemical methods. In PVD a transfer of material is done from a reservoir to the substrate, by changing its physical state (ex.: sputtering, vacuum evaporation). In chemical methods which can be based on gas or liquid phase, a reaction between two components must occur for the film to form (ex.: chemical vapor deposition, spray pyrolysis) [1]. Nowadays, there is a constant pursuit from the semiconductor industry to discover and/or optimize ways for depositing thin films in a simple, cheap, large scale and quick way. Although PVD is often associated with better thin film quality, it needs expensive instruments and uses sophisticated processes to achieve them. Spray coating (a liquid phase chemical method) is able to answer all the above referred needs and still produce high quality layers of different materials.

CSC technique was first used to deposit thin films of CdS in 1966 [2]. Since then, several studies have been conducted on the deposition of different types of materials, such as metal oxides, single, binary and ternary chalcogenides or adamantine copper compounds. Virtually every material can be deposited by this technique, as long as a precursor salt is available [1], [3]. Also, thin films can be easily doped with the desired compound, by adding it to the precursor solution [4]. This technique has been used industrially in glass production and solar cells [5].

The reason this technique has attracted so much interest by researchers of different fields is its simplicity and low-cost processing, as it can be performed in ambient conditions (no vacuum systems required), using cheap equipment fairly easy to handle [3]. Even though no high quality substrates or precursors are required [6], good quality and uniform films can be obtained. The films' final characteristics can be easily controlled by changing the deposition parameters, making it possible to adapt the results to the desired application [4]. On the other hand, CSC setup could be scaled for large depositions, which is an essential characteristic for transitioning to industrial applications, where larger substrates are often used.

However, CSC still faces some challenges. All the reactants must be able to coexist in the same solution, which also means they must be soluble in the same solvent. Differences in solubility can cause phase segregation for multicomponent materials [3], as the solution is not stable enough. Also, morphology of the film greatly depends on the parameters applied, which might be a problem considering the amount of variables involved.

A typical CSC system is composed of a set of components (see Figure 2.1):

- **Precursor solution dispenser**, with a flow-rate controller device to precisely know the amount of solution used;
- **Nozzle**, where the liquid solution is converted into an aerosol. There are different kinds of nozzles being used, such as air blast, ultrasonic and electrostatic [5]. The nozzle could also be associated with a mechanical apparatus that would move it according to specific patterns, designed to create a more uniform layer.
- **Inert Air Compressor**, where, in the case of an air blast nozzle, an inert gas flow at a

determined pressure is connected to it, in order to turn the liquid solution into an aerosol.

- **Hot plate**, where the substrate is placed and can be heated, until the temperature required for the precursors to react and for the solvent to evaporate.
- **Thermocouple**, used to measure the temperature of the hot plate. It is usually connected to a temperature controller, whose function is to keep the temperature at the desired levels.

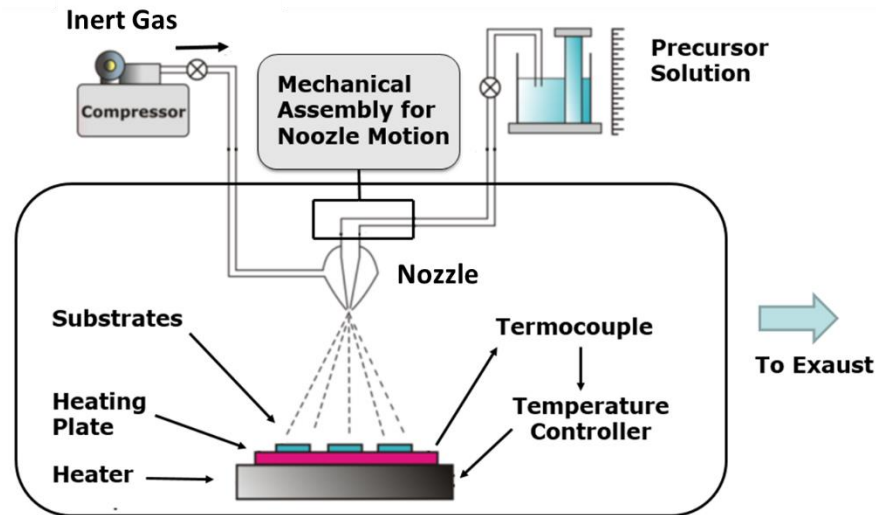


Figure 2.1 – Schematic of a typical CSC setup, including possible components, adapted from [1].

In the CSC process, a precursor solution and compressed inert air travel through a set of small tubes until they reach a nozzle, where the liquid is pulverized, so that it arrives to the substrate in the form of small droplets. The substrate could be heated to potentiate a chemical reaction, occurring between the solution's constituents with the objective of forming a thin film of the desired compound. The temperature of the hot plate is set, controlled and maintained by a thermocouple and a temperature controller. Every other product of the reaction should be volatile, so that it can be extracted (exhausted) from the deposition site [4].

Several parameters can be controlled in the system, such as substrate temperature, air pressure, solution flow-rate, precursor solution composition, deposition time, nozzle distance to substrate (its height) and nozzle positioning and/or motion, in order to obtain films with the specified characteristics. Of those, substrate temperature has been considered one of the most important parameters [6], as it influences solvent evaporation, droplet impact with consecutive spreading, and precursor decomposition [5], all essential processes in CSC. Substrate temperature can change the films' characteristics, causing different optical and electrical behavior. Also, the compositional choice of the precursor solution plays an important role in the final product obtained, as the pH and the oxidation states of the salts chosen influence the structure and morphology of films [5]. Therefore, the effect of these factors must be taken into account when optimizing the thin film deposition of a new material.

2.1.1. Spray Coating vs Spin Coating

Spin-coating deposition method is also a liquid phase chemical deposition technique, based on the use of a precursor solution, such as CSC. Its functionality is based on the placement of the substrate in a rotating device. Drops of solution are put on top of the substrate, which is then set to rotate at a defined speed, for a determined time. The substrates are usually dried and heated after this process, to help evaporate the remaining solvent and enhance film formation [7]. Therefore, it is also a simple and easy process to work with, like CSC, while achieving consistent results of thin and uniform layers.

However, only about 10% of the solution placed on the substrate is actually used, as most of its volume is wasted upon rotation. Also, this method is not suitable for roll-to-roll adaptation, since only one substrate at a time can be placed in the system [8]. Therefore, while spin-coating might achieve very high quality layers of different materials, such as SnS [9], these disadvantages make it unsuitable for

industrial application. Since CSC does not present this kind of drawbacks, it is interesting to compare the quality of thin films obtained by these two techniques.

2.2. Oxide Semiconductor Materials for TFT application

Oxide semiconductor materials have been under the researchers' focus for the past 10 years, as they provide the possibility of fully transparent applications, such as heat insulation films, solar cells and transparent displays [10]. Zinc oxide, tin oxide and indium oxide are among the most explored, due to their sufficiently large band gap ($> 3.1 \text{ eV}$), high carrier density ($> 10^{19} \text{ cm}^{-3}$) and good mobility values ($> 1 \text{ cm}^2/(\text{V}\cdot\text{s})$). However, even though these materials work properly as semiconductors, they can't reach the conductivity values of conductors (up to $600,000 \text{ S cm}^{-1}$ for copper), which presents itself as an obstacle to the goal of designing fully transparent electronic devices [11].

ZnO is among the most explored oxide materials, with broadly available literature on its properties, production and applications [11]–[20]. ZnO films have been fabricated by several groups, using a number of different deposition technologies, such as sputtering [21]–[23], pulsed laser deposition [24]–[26], chemical vapor deposition [27]–[29] and also solution based methods such as dip-coating [30], [31], spin-coating [32] and spray coating [33], [34]. The thin films are uniform and polycrystalline, and even though some of its processing methods do not require temperature, usually the substrate is subjected to heating during deposition or post-annealing. TFTs based on spray-coated ZnO present reported values of mobility between 0.2 and $15 \text{ cm}^2/(\text{V}\cdot\text{s})$ [35], [36].

2.3. Chalcogenides as High Performance Switching Materials

As the silicon-based electronic devices are more and more miniaturized, reaching the limit of Moore's Law, the scientific community started to seek for new materials. Graphene has attracted a lot of attention, as it is the strongest known material to date, it is stretchable, transparent, impermeable, and it has the highest intrinsic electron mobility ever registered, about 100 times the one of silicon [37]. However, it lacks a band gap, being unsuitable for digital electronic applications, as it cannot fully function as a semiconductor [38], or for solar cell applications [39], [40]. Without having this limitation, boron nitrides, metal chalcogenides, oxides, hydroxides and oxychlorides have all been explored as electronic materials. Of these kinds, chalcogenides have shown good promise, due to their high mobilities and air stability. Chalcogenides are composed of a transition element and a chalcogen (elements from group 16 of the periodic table) [38].

Molybdenum and tungsten based chalcogenides are the most studied for field-effect transistors (FET) application, presenting band gaps from the visible to the near-infrared [38]. When applied to FET structures, MoS₂ based devices show mobilities in the order of $200 \text{ cm}^2/(\text{V}\cdot\text{s})$ and large on/off ratios ($\sim 10^8$) [41]. PbS has also been applied to TFTs, with mobilities in the order of $0.09 \text{ cm}^2/(\text{V}\cdot\text{s})$, when deposited by chemical bath deposition [42]. Ti, Sn and Zr based chalcogenides are also indicated as promising semiconductors, but haven't been much explored to this day [38].

2.3.1. Tin Sulfide

SnS compounds have recently attracted attention due to their promising applications in optoelectronics and photovoltaics. SnS presents a band gap on the order of 1.3 eV [43]. It has been reported to be p-type in thin film form [44], with a resistivity of $32.9 \text{ }\Omega\cdot\text{cm}$ and an absorption coefficient of around 10^4 cm^{-1} [45]. The toxicity of other materials used in the photovoltaics field, such as Cd, and the scarcity of Te, In and Ga (present, for instance, in CdTe and CuInGaS₂), has motivated a search for an alternative earth-abundant, non-toxic and inexpensive material [45], [46]. Even though SnS responds to these demands and it is, theoretically, a good material to apply in solar cells due to its high absorption coefficient, the latest reports have not reported efficiencies higher than 3.88% [47]. Nevertheless, SnS is a relatively unexplored material, so there is still much room for improvement and discovery of new applications for this semiconductor.

The growth of SnS thin film using spray pyrolysis technique has been reported by several research

groups, where the effect of growth temperature and the tin and sulfur precursors ratio in the initial solution is reported [43]–[45], [48]–[54]. Usually stannous chloride (SnCl_2) is used as a tin precursor and thiourea ($\text{CS}(\text{NH}_2)_2$) as a sulfur precursor, even though SnCl_4 and variations of substituted thiourea have been tried (such as N,N – diethyl or N,N – dimethyl thiourea). As solvent, water is the most used.

The substrate temperature was reported as the most influential parameter in SnS spray coating, since it greatly affects the films' phase composition, an important property, as each phase has different characteristics. It has been reported that tin monosulfide (SnS) can be achieved at temperatures between 300 and 375°C, being 350°C the temperature at which the film is SnS abundant. The precursor ratio has also been reported to influence the phase composition. While most studies use the 1:1 ratio, Sajeesh et al. [52] have tested solutions with 1:1, 1:2, 1:3 and 1:4 ratios at different temperatures, concluding that the 1:2 ratio solution produced the most stoichiometric solutions for $T=350^\circ\text{C}$, possibly due to sulfur evaporation potentiated by the substrate temperature.

Even though the application of SnS in functional devices, such as TFTs, is still relatively unexplored, spin-coated p-type SnS films photocurrent response was recently studied, where a clear response to incident light is recorded [55]. Also, some reports on SnS_2 , another phase of tin sulfide, have recently come out. U. Zschieschang et al. studied TFTs based on SnS_2 deposited by chemical vapor transport, achieving mobility values of $0.04 \text{ cm}^2/(\text{V}\cdot\text{s})$ and on/off ratios close to 10^6 [56]. SnS_2 in the form of a single layer obtained by mechanical exfoliation was applied as a semiconductor in a TFT structure by D. De et al., presenting high mobilities up to $1 \text{ cm}^2/(\text{V}\cdot\text{s})$ and on/off ratios in the order of 10^6 [57]. Photo detection capabilities were also checked by Y. Huang et al. group, showing efficient phototransistor behavior, even though the response time to pulsed radiation could be improved [58]. Even though other similar studies on SnS_2 are available in the literature [59], [60], studies on SnS are still limited, leaving much room for further improvements.

2.4. Thin-Film Transistor: A Brief Overview of Device Characteristics

Thin-film transistors are field-effect devices working as switches and amplifiers, used in digital and analog electronics, especially flat panel displays. The field effect device was first described in the 30s in a patent by Lilienfeld, which was followed by Heil's and Shockley's, who described in more detail the operation and structure of the devices [61]. TFT technology was applied into a working device based on CdS in the 60s, but its research was laid aside due to the increasing interest in the Metal Oxide Semiconductor Field Effect Transistor (MOSFET) technology. It was only in the end of the 70s, with the study of amorphous silicon on TFTs to be applied as switches in LCDs, that subsequent investment in this field of research was done [61]. Recently, transparent, flexible and/or stretchable electronics are being explored, with the introduction of oxides and organics as semiconductors, aiming for wearable gadgets and smart applications.

TFTs are fabricated using thin layers of material and follow the same working principle as MOSFETs. It also has three terminals (gate, source and drain), where the drain and source electrodes are connected to the semiconductor layer, which is isolated from the third terminal, the gate, by a dielectric. The basic operation principle of the TFT is gate modulation of the current flowing between drain and source, which determines if the transistor is on or off [62]. The TFT can be fabricated in different configurations according to the place where the layers and terminals are: they can be top-gate or bottom-gate, and, among these, staggered or coplanar. The choice of configuration is based on the fabrication requirements and the final application. Also, depending on the type of polarity, n-type or p-type, and the value of the threshold voltage, V_T , the TFT can also be classified in enhancement or depletion mode devices: for an n-type device V_T is positive or negative, respectively, the opposite applies for p-type transistors [63].

TFTs can be working in one of the following three states:

- **OFF State**, if the drain voltage is zero, $V_D = 0V$, as negligible current is flowing between drain and source, I_D , regardless of the gate voltage, V_G ;
- **Linear or triode mode**, if $V_D > 0V$ and $V_D < V_G - V_T$, in which case I_D can be defined by

$$I_D = C_i \mu_{FE} \frac{W}{L} \left[(V_G - V_T) V_D - \frac{1}{2} V_D^2 \right] \quad [2.1]$$

Where C_i is the dielectric capacitance per unit area, μ_{FE} is the field-effect mobility, W and L are the width and length of the semiconductor channel, respectively, V_G is the gate voltage and V_T is the threshold voltage. When $V_D \ll 0$ V, the quadratic term of the equation can be neglected, resulting in a linear relation between I_D and V_D , as a result of a uniform distribution of charges across the channel.

- **Saturation**, if $V_D > 0$ V and $V_D > V_G - V_T$, in which case I_D can be defined by

$$I_D = C_i \mu_{sat} \frac{W}{2L} (V_G - V_T)^2 \quad [2.2]$$

Where μ_{sat} is the saturation mobility. When approaching the $V_D = V_G - V_T$ point, the semiconductor channel depth decreases near the drain terminal, increasing the channel resistance, which is usually called the pinch-off point. After this point, I_D is no longer dependent on V_D and eventually stabilizes (saturation).

These operation modes are usually described using characteristic curves (see Figure 2.2), such as output and transfer curves. Several characteristic parameters can be taken from these curves, like the ratio between on- and off-current, V_T , V_{ON} , mobility (either field-effect or saturation) and the subthreshold swing (SS) [64].

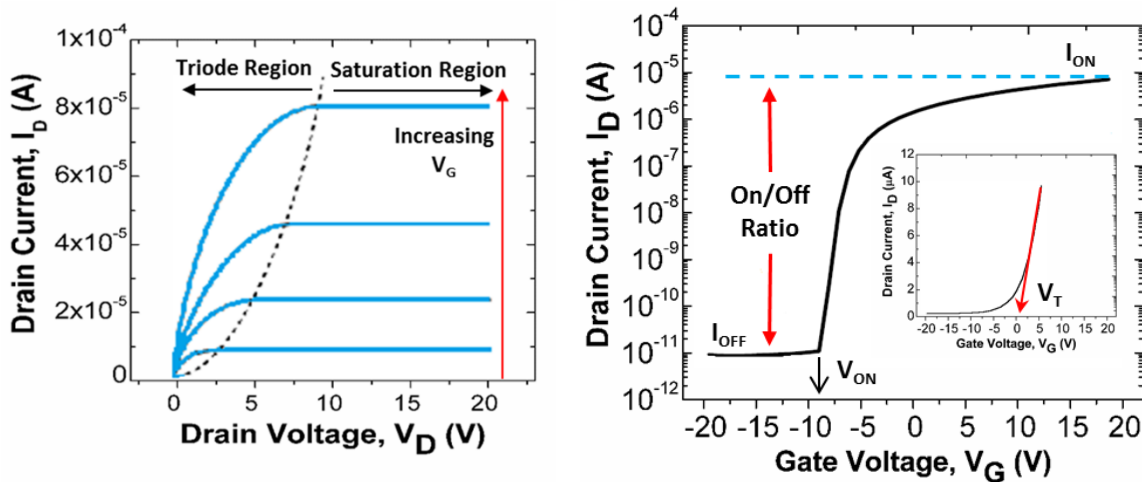


Figure 2.2 - Characteristic curves of a TFT, with the output curves on the left and the transfer curves on the right. Adapted from [65] and [63].

2.4.1. Phototransistor: A Device for Light Detection

As one of the chosen semiconductors was photosensitive, a phototransistor was fabricated in this project. The invention of these devices is often attributed to John N. Shive of Bells Labs [66]–[68], shortly after the first transistors were invented during the late 1940s, using a germanium point-contact transistor. Even though the first application tested was its integration in a component of the telephone, the phototransistor would eventually emerge as a television and video-imaging technology[68].

A phototransistor is a three-terminal switching device that relays on the exposure to light to operate, which causes variations of current that can be measured. Photodetection occurs due to the photogenerated carriers that are formed when the energy of a photon is equal or higher than the material's band gap, allowing an electron to move from the valence to the conduction band. These carriers are originated in the semiconductor channel in addition to the ones solely created by the applied electric field between the channel and the gate oxide [69]. In spite of their lower response times, phototransistors are considered to be more sensitive when compared to photodiodes (another photodetector device, based on a two terminal diode). They can be wired in specific configurations, allowing it to work as a light-to-voltage converter [70].

Nowadays, light detectors, such as phototransistors, find high revenue applications in smartphones, tablets and computers, where UV, RGB and pulsed light sensors are applied [71]. The unit demand in the industry has been rising and it is estimated to follow the same tendency in the next few years (Annex A). More recently, research has been focusing on phototransistor implementation on large arrays for imaging applications, where large-area detectors for use in medical radiography have been investigated [72].

3. MATERIALS AND METHODS

In this section, a detailed description of the solutions, substrates, equipment and techniques used to deposit films, characterize and test them on devices is made.

3.1. Precursor Solutions

A 0.1M solution of zinc acetate ($\text{Zn}(\text{CH}_3\text{COO})_2$ - Sigma Aldrich with 99.99% purity) dissolved in methanol (CH_4O) was used for deposition of the ZnO films.

Solution X was used to deposit Oxide X. The concentration of the solution was controlled by adding solvent provided by the manufacturer of Solution X. It was considered that the volumetric density of Solution X and Solvent X were the same.

For the deposition of SnS, a mix of two precursor solutions was made. Firstly, a 0.1M of tin (II) chloride dehydrate ($\text{SnCl}_2 \cdot 2\text{H}_2\text{O}$ - Sigma Aldrich with 99.99% purity) solution was made by dissolving the salts in methanol. As the $\text{SnCl}_2 \cdot 2\text{H}_2\text{O}$ salt dissolved tends to form a precipitate ($\text{SnCl}_2(\text{aq}) + \text{H}_2\text{O}(\text{l}) \rightleftharpoons \text{Sn}(\text{OH})\text{Cl}(\text{s}) + \text{HCl}(\text{aq})$), a few drops of HCl were added to prevent this effect. Secondly, thiourea ($\text{CH}_4\text{N}_2\text{S}$ - Merk with a 99% purity) was dissolved into methanol in order to obtain a concentration of 0.2M. A volume of 10 mL was prepared for both solutions and they were both kept stirring until the salts were completely dissolved. Finally, the solutions were mixed (10 mL of each) and stirred, making the final mix ready for application.

3.2. Substrates

P-type silicon wafers with a {111} crystal orientation coated with photoresist were used for film optimization tests. The wafers supplied were cut into individual pieces of 1.75x1.75 cm. The layer of photoresist worked as a protective layer, keeping the samples as clean as possible. So, prior to sample use, the photoresist was removed from each individual sample, using acetone and isopropanol. To enhance the substrate's cleanness, the samples were placed on a UV/Ozone PhotoReactor (model PR-100 from UVP.inc) for 5 minutes.

For the TFT testing, pre-made commercial n-type Si substrates with a {111} crystal orientation were used. The wafers supplied were cut into individual pieces of 1.75x1.75 cm. The substrates contained a 210 nm SiO_2 layer as dielectric across in the entire wafer. The S/D electrode layers consisted of a 2 nm Ti layer on the bottom (for enhanced adhesion) and 50 nm layer of gold on top, defined by conventional photolithography, using the mask that can be consulted in Annex B. The substrates were supplied already with those layers deposited, so the semiconductor layer was deposited on top. A lateral view of the device structure can be seen in Figure 3.1. Although the used mask allowed the choice among different transistor configurations, after the initial experiments, the chosen layout was the ring transistor, yielding TFTs with W of 1000 μm and L ranging between 10 μm and 40 μm . The current was set to run from the inner electrode to the outer electrode (as can be seen in Figure 3.1). The referred choices will be explained in section 4.1.2.

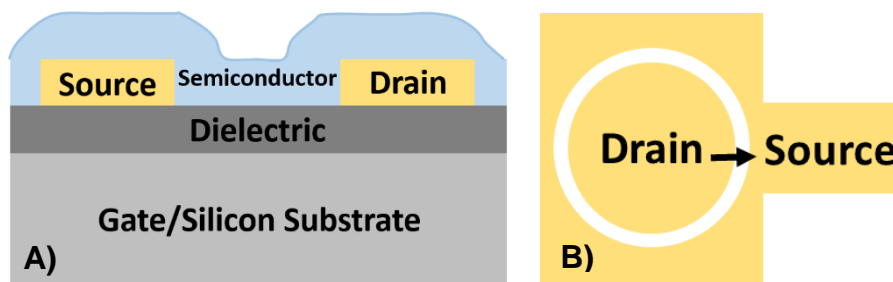


Figure 3.1 – Schematic of the TFT devices structure. **A)** Transversal view. **B)** Top view of a ring transistor. The arrow represents the direction of current set for these devices throughout the entire project.

3.3. Thin Film Deposition Methods

The main focus of this thesis was the implementation and optimization of a CSC system (**Figure 3.2**). Even though it was homemade, most of its components had already been used in previous work, reported by Andringa et al. [73]. Modifications in the precursor solution dispenser were made to ensure a controlled flow-rate and to study its influence. This comprised storing the solution in a syringe during deposition, to prevent solvent evaporation, and installing a syringe pump to precisely control the amount of sprayed solution. However, at the beginning and end of deposition, the FR seemed to be irregular (discontinuous spraying). So, an improvised shutter (placed between the nozzle and the substrate), consisting on a glass barrier attached to a universal support, was implemented. All the other instruments (heater, thermocouple, nozzle, rotational mechanical motor and air pressure controller) had already been used in the previous experiment mentioned above.

The chosen nozzle (a Meinhard Nebulizer TR-30-A3) was connected to a nitrogen air flow at a constant pressure of 1 bar and to the syringe pump (Havard Apparatus 11plus), from where the solution was injected at a determined flow rate (FR), ranging between 0.1 and 3 mL/min. The nozzle's mechanical rotation motor system (Maxon) and powered by a power supply (Delta Electronika) at a constant voltage of 1 V, was implemented to ensure better uniformity of films, which kept the rotation speed and radius constant throughout the experiments. The substrates were placed on a heater (Ceran 500 11A controlled by a Eurotherm system), maintained at constant temperature (T), ranging between 30 and 400°C, depending on the experiment ($\pm 5^\circ\text{C}$). Nozzle height (H) values were varied between 5 and 11 cm and deposition time (t) between 15 and 120 s. The specific parameters used for each experiment will be stated in the respective results section.

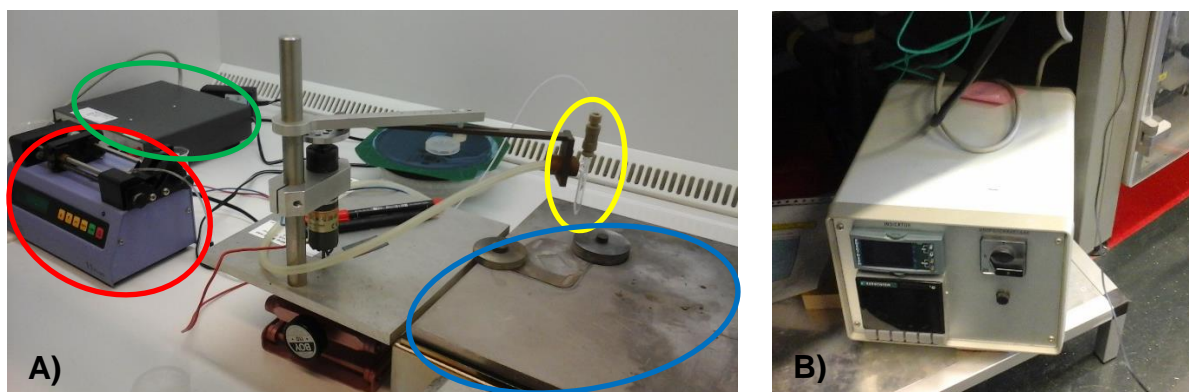


Figure 3.2 - Implemented CSC system. **A)** Setup placed inside the fume hood: Power supply for the mechanical rotation motor system (green), syringe pump (red), nozzle (yellow) and hot plate (blue). **B)** Temperature controller device.

For spin-coating deposition, a ATMsse OPTIspin SB20 spin coater system was used to make the standard layers and devices. The rotation speed was maintained at 3000 rpm and time the time at 30 s, according to previous tests made by a Holst Centre team.

3.4. Characterization Methods

Film thickness and roughness in layers deposited onto Si substrates were measured by a DektakXT profilometer, equipped with a 12.2 μm tip. The samples were scratched with a surgical blade and the step between the scratch and the film was measured in order to determine the films' thickness. Although this technique proved to be sufficient with film thickness higher than 20 nm, for thinner films the scratches were not very well defined, making it impossible to accurately do the measurements. Optical observation and image caption was done with a Leica Microscope.

Scanning electron microscopy (SEM) was used for evaluation of the surface morphology of SnS films, using a Zeiss Auriga crossbeam. Given the reduced thickness of the films a low accelerating voltage was used (1 keV), together with in-lens secondary electrons detector. Elemental analysis of the same

Spray Coating of Oxide and Chalcogenide Semiconductor Layers for TFT Application

films was obtained by energy dispersive X-ray spectroscopy (EDS) using a Oxford XMax-150 detector (inside Zeiss Auriga) with AZTec software. Analysis was carried out using accelerating voltage of 15 keV and aperture size of 60 μm to assure good compromise between x-ray signal and spatial resolution.

For the electrical characterization of the TFT substrates, consisting of transfer and output characteristics, Hewlett Packard 4155B Semiconductor parameter analyzers was used, with Cascade Microtech M150 manual probe stations, placed inside a glove box from MBraun (MB 200B), where the atmosphere was controlled, preventing the presence of oxygen or water in the air. To extract and analyze the data, Agilent Desktop Easy Expert software was used.

The phototransistors were tested with yellow light (wavelength of about 570 nm), with 100 W maximum electrical power, built in the Leica Microscope of the probe station. Complementary testing to the device was done with a single IR LED, with a wavelength of 850 nm.

4. RESULTS AND DISCUSSION

4.1. Zinc Oxide Standard Experiment: Spray Coating System Optimization

As previously mentioned in section 1, the CSC technique was relatively new in the Holst Centre. So, before the start of the project, it was necessary to assemble and test the system to ensure its functionality. Also, some changes had to be implemented, to maximize the quality of the final thin films. For controlled flow rates and precise deposition times, a syringe pump and a shutter were added.

4.1.1. Zinc Oxide Thin Films

ZnO thin films were chosen as a standard experiment due to the availability of reports found in literature and also because a similar study had been conducted previously in the Holst Centre, with the goal of achieving a NO₂ gas sensing device [73]. Most of the deposition conditions, such as the temperature of 400°C, the precursor solution (0.1M of zinc acetate in methanol) and the deposition time (1 minute), were established based on that project. However, some parameters had to be experimented and optimized. To study the FR, the nitrogen pressure was set to 1 bar and the H to 5 cm. Different values were tested (0.1, 0.2, 0.5 and 1 mL/min), keeping the deposition time at 1 minute, with the objective of getting even and good quality films. Smaller FR of 0.1 and 0.2 mL/min produced very thin films for the fixed t of 1 minute, going against the objective of high throughput, necessary for industrial applications and, therefore, intended for these experiments. On the other hand, roughness in films deposited using 1 mL/min of FR was higher. So, an intermediate value of 0.5 mL/min was used to obtain uniform films and high throughput, achieving film thicknesses of 40 nm.

Then, the deposition time was varied in order to study its influence on the films' quality. A thickness analysis to the films was performed, achieving values between 10 and 90 nm, for t below 120 s. A linear relation between deposition time and film thickness can be made, as seen in Figure 4.1 A. Knowing this relation, it is possible to estimate the layer thickness by choosing a specific deposition time. Also, very uniform structures were obtained, as can be seen by the profiles of Figure 4.1 B, where the roughness is not higher than a few nanometers. These results confirm the possibility of this system to obtain very uniform semiconductor layers and precisely controlled film thicknesses with ZnO.

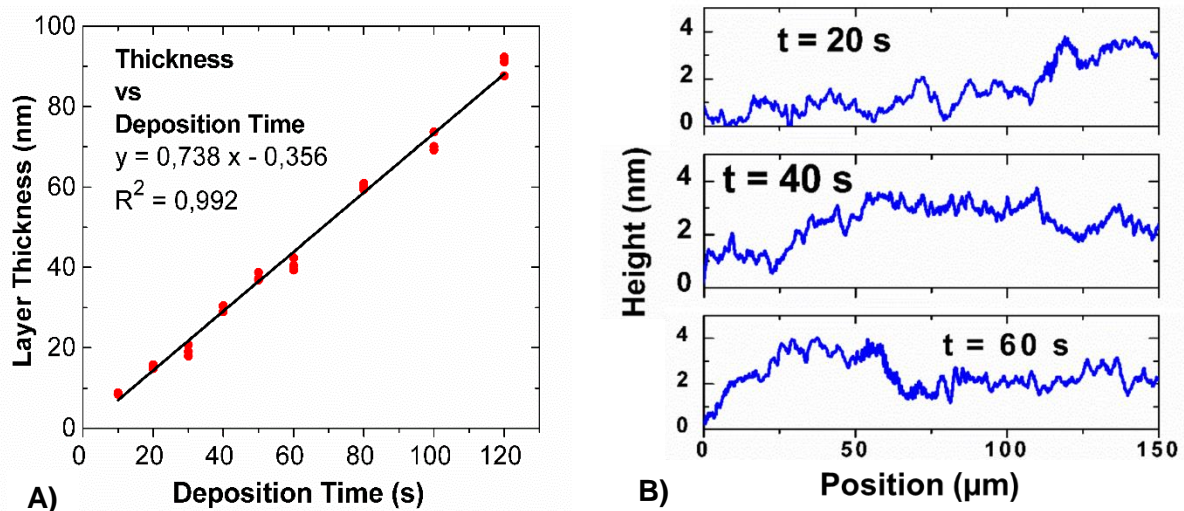


Figure 4.1 - ZnO thin film characterization. **A)** Graph of thin film thickness (nm) dependence on deposition time (s), showing a linear relation. **B)** Profiles of three different films, with deposition times of 20, 40 and 60 s, showing the roughness of the layers.

4.1.2. Thin-Film Transistor Considerations

Over the current study, the semiconductor layer deposited by the CSC technique of the fabricated TFTs was never patterned, for improved throughput. Even though this model of research is suitable for initial

studies, it can also lead to some problems, such as overestimation of field-effect mobility due to fringing electric fields. This effect is reflected on an actual increase of the semiconductor dimensions, namely a larger transistor width than the one geometrically defined by the width of source-drain electrodes, due to peripheral currents (also called fringing currents) [74] (Figure 4.2).

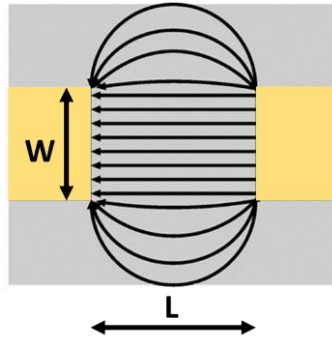


Figure 4.2 - Schematic of the fringing electric field on unpatterned semiconductor layer of a typical TFT architecture. Adapted from [75].

Given this and since the transistor masks available allowed for the choice of different device layouts (as can be seen in Annex B), ring transistors were selected, as they provide a coaxial source-drain layout. This configuration prevents the fringing effect from happening, as long as the current is flowing from the inner contact circle (drain) to the outer contact circle (source) [75]. The same characteristic equations described in section 2 were used, as the device was considered to work similarly to a transistor in a common layout (as seen in Figure 4.2).

Also, as the gate electrode was the silicon substrate itself and due to the non-patterned semiconductor, an important effect of gate modulation, not only between drain and source (as intended), but across the substrate must be taken into account when analyzing TFT characteristics. On the other hand, high drain voltages were used to avoid gate leakage current exceeding drain-to-source current for larger gate voltages, an effect registered in the initial tests, when low drain voltages were applied. Hence, mobility values were estimated using the saturation mode equations (see Annex C for a detailed explanation).

4.1.3. Zinc Oxide Thin Film Transistors

When depositing the optimized thin films (as described in section 4.1.1, with T of 400 °C, FR of 0.5 mL/min and H of 5 cm) on transistor substrates and then annealing them inside the glove box for 30 minutes at 250°C. Transistors with fixed channel lengths of 10 μm and layers with different thicknesses of semiconductor were analyzed, from which the transfer and output curves seen in Figure 4.3 were obtained.

Even though all the analyzed ZnO thicknesses provide noticeable field effect, thinner layers result in lower off-current and V_{ON} closer to 0 V, suggesting an increase in electrical resistivity of the material (see also Table 4.1). This effect might be explained by the typically smaller grain sizes in thinner ZnO films (considering a columnar growth structure) and/or that the amorphous incubation layer is present in most of the films depth, factors that make the carrier transport more difficult. Note that, while the trend of SS with thickness seems to suggest improved interface properties for thinner films, an opposite trend is verified for μ_{SAT} . So, it should be considered that SS is significantly degraded by the larger off-current of thicker films.

Even though the μ_{SAT} values are quite small when compared to some research group's work, such as Fortunato et al., where mobilities of 20 $\text{cm}^2/(\text{V}\cdot\text{s})$ have been achieved on sputtered ZnO TFTs [35], it is important to consider that the non-patterning of the semiconductor and the use of a chemical solution based deposition method might be the cause for these relatively low values. In fact, Bashir et al. [34] have made a comparative study of two different spray-coated ZnO TFT architectures, one with a non-patterned semiconductor on top of the gold contacts and another with patterned semiconductor with aluminum contacts on top. It was concluded that the first device exhibited substantially lower mobilities, in the order of 1.1 $\text{cm}^2/(\text{V}\cdot\text{s})$, while the second showed high values in the order of 15 $\text{cm}^2/(\text{V}\cdot\text{s})$, for

depositions made on a substrate heated to 400 °C. This effect is attributed to the energy offset between the Fermi level of Au ($E_F = 5.1$ eV) and the band gap of ZnO (4.4 eV), as the Fermi level of Al allows for a smaller energy offset (4.2 eV), and also to the different device architectures.

Therefore, the low mobility values of Table 4.1 could be explained not only by the solution based technique used, but also by the choice of TFT architecture, electrode and dielectric (which should be optimized for each device, considering the semiconductor chosen).

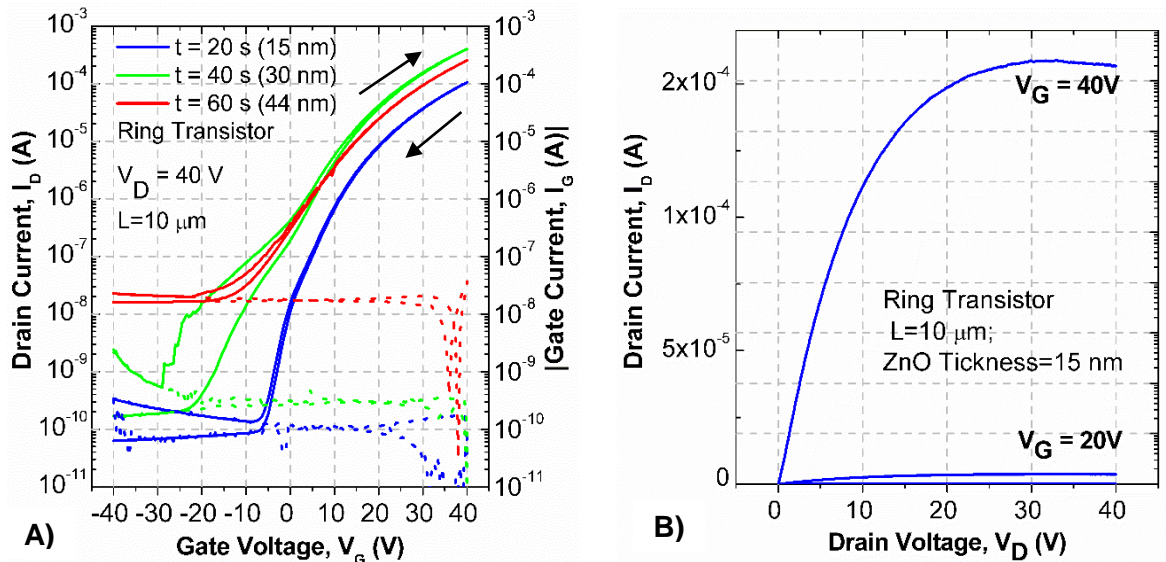


Figure 4.3 – Electrical characterization of the ZnO TFTs. **A)** Transfer curves of ring transistors with three different channel thicknesses. Continuous and dashed lines represent drain and leakage currents, respectively. Arrows indicate the V_G sweep direction, showing a clockwise hysteresis. **B)** Output Curves of a TFT with films of 15 nm.

Table 4.1 – Extrated characteristic parameter values from Figure 4.3 of the produced ZnO TFTs, considering different film deposition times (different thicknesses).

Deposition Time, t (s)	Saturated Mobility ($\text{cm}^2/(\text{V}\cdot\text{s})$)	V_{ON} (V)	Threshold Voltage, V_T (V)	On/Off Ratio	SS (V/dec)
20	5.7×10^{-2}	-6	7.1×10^{-2}	1×10^6	2.5
40	2.3×10^{-1}	-29	8.2×10^{-2}	8×10^5	2.4
60	1.4×10^{-1}	-15	7.7×10^{-2}	1.5×10^4	4.6

In light of the results obtained and of the considerations made, the technique's setup was considered capable of producing uniform and good quality thin films. With these results in mind and knowing the limitations of the methodology employed, the project moved forward to the main experiments, with other materials. This standard experiment was later on performed again every time the results suggested system malfunction in order to confirm its reliability.

4.2. Oxide X Deposited by Spin-Coating and Spray-Coating

In this section, a comparison of two methods for deposition of thin layers, spray coating and spin coating, is presented, while employing the same precursor solution, solution X, to get oxide X semiconductor film. The objective of this experiment was to provide information to a Holst Centre partner about the applications of a commercial solution that had been developed at the time for spin-coating, by assessing if it was suitable for spray-coating deposition. One of the requirements of the partner for this project was the use of substrate temperature while spray-coating below 100°C.

After deposition, every thin film was annealed two times, according to the procedure developed for spin-coated films. The first one, a soft-annealing, was performed at 250 °C for 30 minutes, while the second, a hard-annealing, was done at 350 °C for 1 hour. These annealing procedures were done to mimic the conditions of the substrates produced by deposition of the two different techniques, so that they could be easily compared. The transistor substrates were also subjected to a 10 minutes UV curing, done before the two annealing steps, in order to improve the material's conductivity.

4.2.1. Oxide X Thin Film Optimization

Knowing this material had never been deposited by CSC technique and considering it is an oxide, the first tests were based on the experience acquired from the section 4.1.1. The goal at this stage was, by applying different processing conditions and analyzing the optical images and profiles of the samples deposited on Si, to reach an optimal set of parameters that would result on the deposition of homogenous films. After each attempt, an optical image and the profile of the sample were taken to determine if the experiments were moving forward in the right direction, as can be seen in Annex D. From now on, samples will be named using their respective serial number.

Since the solution was firstly optimized for spin-coating, the first assumption made was that it might be too concentrated for spray-coating, so in the initial tests low flows (0.1 mL/min) and low deposition times (15 and 30 seconds) were used. Also, a near-ambient substrate temperature of 40°C for deposition was chosen to match spin-coating conditions, while keeping H at 5 cm. A1 images and profiles show that this set of parameters results on the formation of material accumulations, which are intensified with the increase in deposition time, as seen in A2 (see Annex D).

Since increase in temperature generally causes an improvement of film uniformity, the goal of the second set of samples (B1, B2, B3) was to study the substrate deposition temperature effect on the films (T of 40, 60 and 80°C were used). Also, in an attempt to redistribute the material accumulations throughout the film, the FR was increased to 0.5 mL/min. However, this approach caused even higher irregularities and uneven films, as can be seen by the material peak of 3500 nm height present in the profile of B3.

The third set of samples was made returning to near-ambient temperatures (40°C) and diluting the initial solution used, mixing one part of Solution X and three parts of solvent (1:3 solution). The most uniform sample seemed to be C2, but, when repeating the deposition under the same conditions, irregular films were obtained, showing important issues of reproducibility.

After trying different combinations of parameters without success, the nozzle height influence was tested on Set D, keeping near-ambient T of 40°C, FR of 0.1 mL/min, t of 20 seconds and using the 1:3 solution. As can be verified by the optical images and profiles of Figure 4.4, the films uniformity seems to improve as the height increases. Irregularities of the sample with H=5 cm are visible and reach about 200 nm of height. These values drastically decrease when H is set to 11 cm, for which the irregularities can no longer be seen in the sample, as confirmed by its profile (height differences of less than 5 nm). This effect might be explained by the smaller droplet size of the spraying at the substrate level for higher H, resulting in a uniform material distribution on the substrate.

However, at this point, film presence was not possible to confirm, as film thickness measurements (done as described in section 3.4) couldn't be accurately made (the scratch done did not show a step like design, as it did with the ZnO films). So, set E of samples was made, where the deposition time influence was studied (t values of 40, 60 and 120 s), keeping H at 9 cm, T at 40°C and FR at 0.1 mL/min, which

only caused the reappearance of irregularities in the film, thus the deposition time was kept at 20 seconds for future depositions and H at 11 cm to guarantee the most uniform layers possible. Film presence was later on confirmed with transistor structures as explained in the next section.

Increasing Nozzle Height

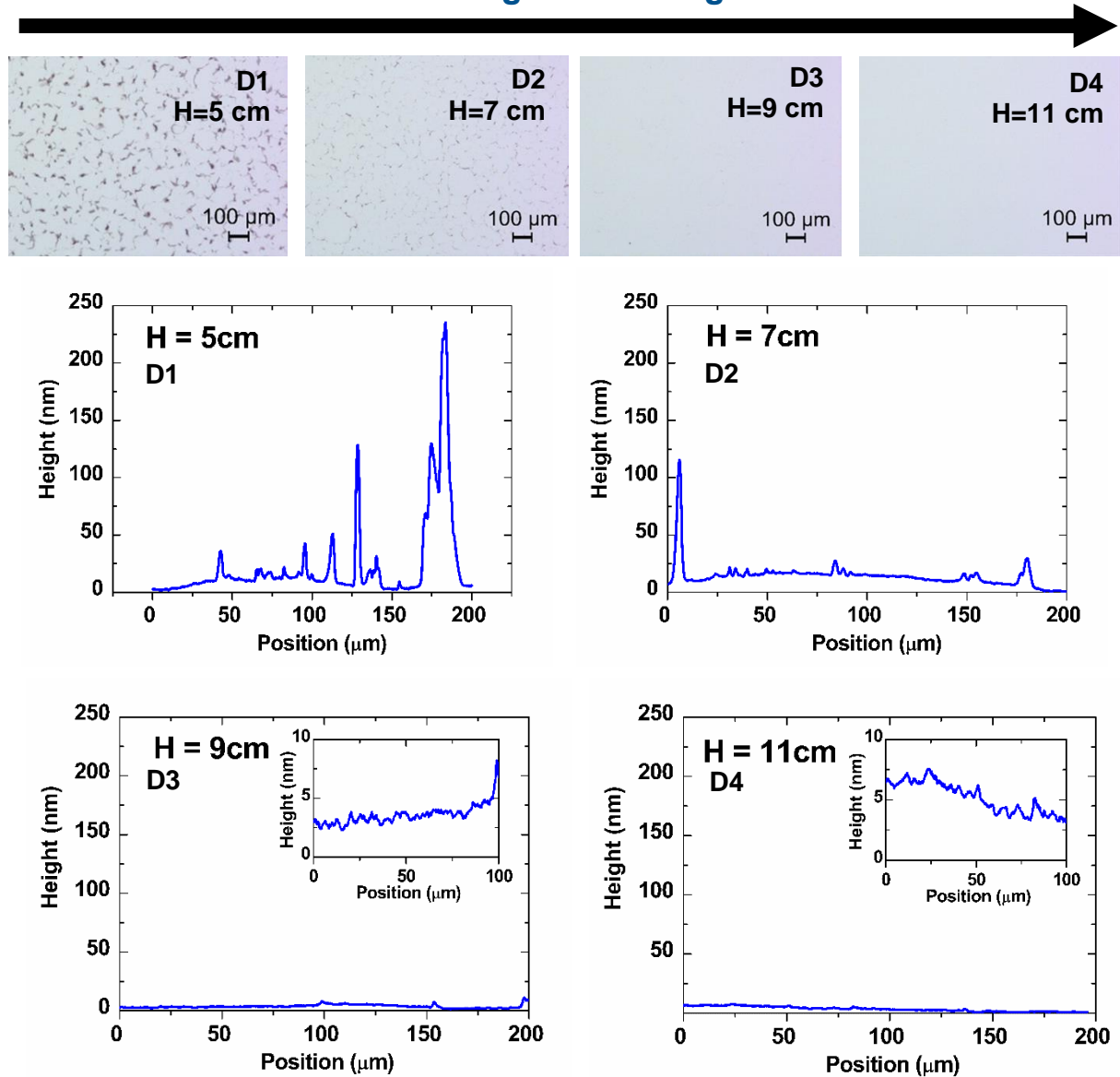


Figure 4.4 – Optical images (on top) and film profiles (on the bottom) of oxide X samples deposited using different nozzle heights, of 5, 7, 9 and 11 cm, for samples I1, I2, I3 and I4, respectively.

4.2.2. Oxide X TFTs: performance comparison between the two techniques

The previously optimized spray-coated Oxide X D4 thin films (H=11 cm) were deposited on transistor substrates, in order to confirm the films' presence and compare, by analyzing the TFT behavior, spin-coated and spray-coated films. It is necessary to consider that the spin-coating deposition of the Solution X had already been optimized by another Holst Centre team (see parameters in section 3.3). No changes were made to the processing by this technique, as the main focus was the CSC. As can be seen in Figure 4.5, silicon dioxide below the spray-coated Oxide X enhances the presence of coffee-ring structures, probably shaped according to the size of the spray's droplets and by the slow solvent evaporation, happening due to the low substrate deposition temperature used. The film made with spin-coating does not show this effect, looking uniform and free of film irregularities.

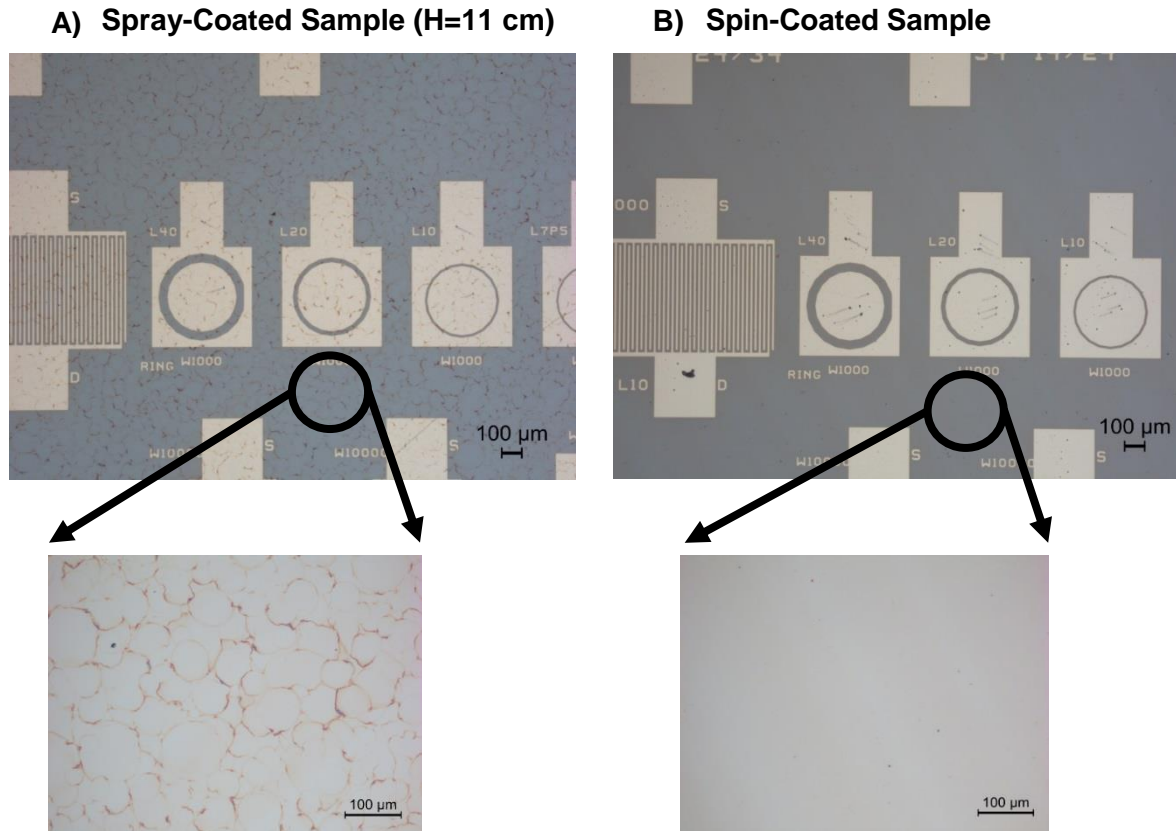


Figure 4.5 - Optical images of oxide X films deposited on transistor substrates. **A)** Using spray-coating with a fixed nozzle height of 11 cm. **B)** Using spin-coating.

When extracting the TFTs transfer curves (Figure 4.6), a clear confirmation of the presence of Oxide X layer on the transistor substrates can be drawn. Therefore, the spray-coated Oxide X thin films can be applied as semiconductor layers of TFTs, producing functional devices.

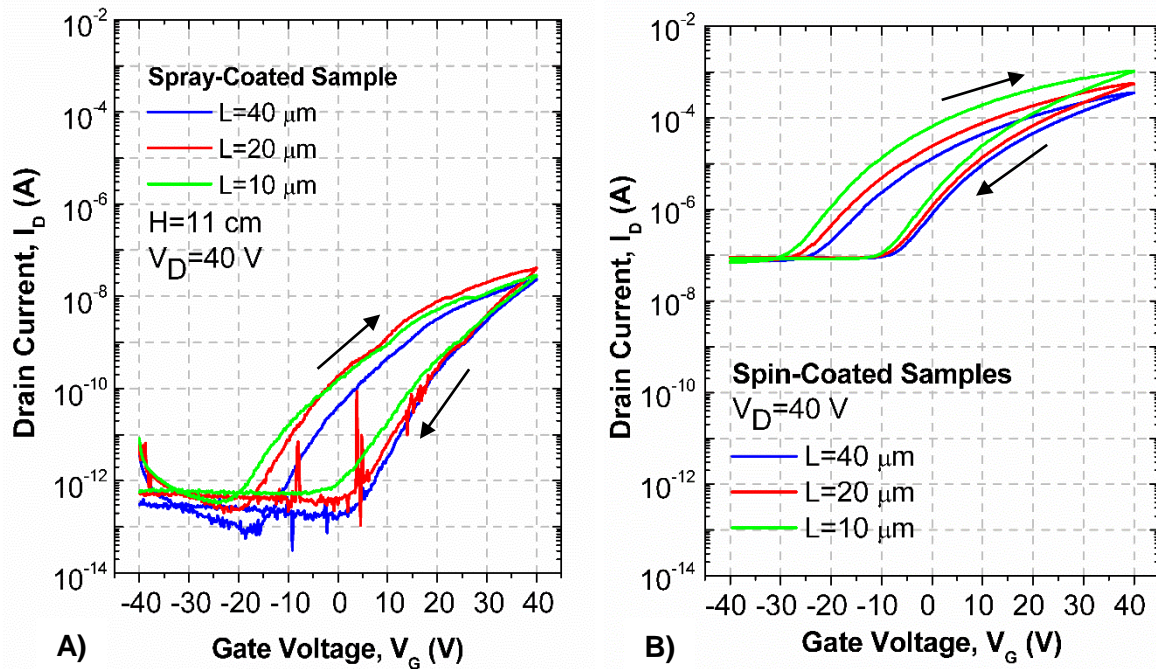


Figure 4.6 - Electrical characterization of the Oxide X TFTs with L of 40, 20 and 10 μm . **A)** Transfer curves of spray-coated TFTs. **B)** Transfer curves of spin-coated TFTs. Arrows indicate the V_G sweep direction, showing a clockwise hysteresis.

Spray Coating of Oxide and Chalcogenide Semiconductor Layers for TFT Application

Very different results can be observed in both graphs, explained by the lower on and off currents present in spray-coated TFTs, which leads to lower mobility values and overall inferior results (Table 4.2).

Table 4.2 – Extrated characteristic parameters from Figure 4.6 of Oxide X TFTs when deposited by spin-coating and spray-coating, considering transistors with different channel lengths.

Deposition Method	Channel Length (μm)	Saturation Mobility ($\text{cm}^2/(\text{V}\cdot\text{s})$)	On/Off Current Ratio	V_{ON} (V)	V_{T} (V)	SS (V/dec)
Spin-Coated	40	2.4	4.3×10^3	-25	-2.4×10^{-1}	6.1
	20	1.9	7.1×10^3	-28	-1.5×10^{-1}	6.7
	10	1.7	1.3×10^4	-31	-6.8×10^{-2}	6.1
Spray-Coated	40	4.0×10^{-4}	2.0×10^5	-15	-9.1×10^{-2}	3.8
	20	3.0×10^{-4}	2.0×10^5	-19	-8.0×10^{-2}	4.3
	10	1.2×10^{-4}	7.5×10^4	-21	-8.8×10^{-2}	3.9

As the composition of this oxide semiconductor layer is unknown, generic reviews among the oxide based TFTs were consulted, in order to perform a critical analysis of the exposed results. Frenzel et al. review on transparent TFTs (where oxides are used as channel materials) explores the published work on this field of research between 2003 and 2013, considering different semiconductor deposition techniques and different device structures [76]. According to the compiled data, mobilities of oxide based TFTs are reported to be between 0.02 and 107.8 $\text{cm}^2/(\text{V}\cdot\text{s})$, with on/off ratios lying in the range of 10^1 - 10^9 with subthreshold swings (SS) of 80-4000 mV/dec, depending on material selection, deposition technique, (post-)processing parameters and device structure, showing a broad range of performance variation among this technology.

Fortunato et al. group collected information related to solution-processed oxides, including deposition techniques, such as spin-coating and spray-coating of different materials, for articles published until 2011 [77]. In the case of TFTs based on spin-coated ZTO, mobilities reported range from 0.76 and 27.3 $\text{cm}^2/(\text{V}\cdot\text{s})$, while the on/off ratios lay between 10^5 and 10^8 . Spin-coated GIZO TFTs present mobilities between 0.05 and 7.65 $\text{cm}^2/(\text{V}\cdot\text{s})$ with on/off ratios in the range of 10^4 - 10^7 . Generally, it is observed that solution-processed TFTs reveal lower mobility values when compared to devices with thin films processed by PVD.

The results obtained in this work follow this trend, achieving performance levels closer to the ones typically found for solution processed oxide TFTs. The coffee-ring topography verified in Figure 4.5 for spray-coated films should be the main responsible for degraded performance when comparing to spin-coated devices, as this creates areas of film with different thickness that interfere with the movement of carriers across the channel layer, due to a larger defect concentration, increasing its electrical resistivity. This is reinforced by the fact that both mobility and off-current are significantly higher for spin-coated TFTs, explained by the device's sensitivity to the electrical resistivity of the semiconductor layer, due to the gate modulation of a large area of the devices and not only between drain and source electrodes (see section 4.1.2).

The effect of L on device properties also reinforces the improved layer uniformity of spin-coated films. As would be expected from equation 2.2, maximum I_{D} should scale with W/L, unless layer uniformity, short-channel effects or contact resistance start to dominate device performance as L is reduced. For

spin-coated samples only a small effect of contact resistance for shorter channel devices is notorious by the small degradation of μ_{SAT} as L decreases. This effect should not be attributed to overestimation of μ_{SAT} for longer L , since the ring transistor layout used in this work inhibits fringing current effects, as mentioned in 4.1.2. Still, maximum I_{D} scales almost perfectly with W/L . On the other hand, for spray-coated samples the evolution of I_{D} with W/L does not appear to follow the same trend, which should be due to the large degree of non-uniformity of the semiconductor films.

Results in Table 4.2 can also be compared with the ones presented in table 4.1, for sprayed ZnO TFTs. Data shows that significantly improved field-effect modulation is achieved with ZnO than with oxide X. In addition to the effects of resistivity and film uniformity mentioned above in the comparison of spin-coated and spray-coated samples, the effect of film thickness should also be highly relevant here. Since it was not possible to accurately determine the thickness of oxide X, results suggest that it should be very low (below 15 nm), possibly even compromising the continuity of the film through all the area between source and drain electrodes, inhibiting significant current modulation with moderate values of V_{G} .

From the obtained results, even if functional spray coated oxide X TFT are fabricated, its deposition conditions and processing certainly need to be tuned, particularly to improve film uniformity.

4.3. Case Study: SnS Thin-Films

In this section, a relatively unexplored material for transistors, tin sulfide, is focused. Firstly, thin film deposition and optimization is done considering the conclusions taken from sections 4.1.1 and 4.2.1. Then, films using the same deposition conditions were applied onto TFT substrates and the device's characteristics measured. Finally, the TFT was exposed to light and the material's photo detection capabilities analyzed.

4.3.1. SnS Thin-Film Optimization

Firstly, several different configurations of precursor solutions were tested. The initial solution used was based on T.H. Sajeesh et al. group's research [52], where the molarity, salts chosen (0.1M of $\text{SnCl}_2 \cdot 2\text{H}_2\text{O}$ and 0.2M of $\text{CH}_4\text{N}_2\text{S}$) and solvent used (deionized water) were mimicked as consulted. However, when tested on our setup, the solution appeared to clog on the smaller tubes, causing obstructions and damaging the system, suggesting that deionized water was not the best solvent. So, a mixture of different proportions of isopropyl alcohol and water were tried, following the work described by N. Koteeswara Reddy et al. [48] and M. Calixto-Rodriguez et al. [45]. As these solvents did not improve the solubility, methanol and ethanol were also tested. While all the other solutions exhibit a yellow coloration, the methanol based one was fully transparent, indicating this to be the best solvent for the used salts (see Annex E). This solution was then tested without any obstruction problem.

For the first tests on the study of the SnS thin films the variation and influence of the solution flow-rate, the deposition time and the substrate deposition temperature were explored. Sample parameters used and respective optical images can be seen in Annex F. From now on, samples will be named using their respective serial number.

In the group of samples F, the FR was studied (ranging from 0.5 to 3 mL/min), keeping T at 250°C and t at 30 seconds. Too much material seemed to be deposited in Samples F2, F3 and F4 (FR of 1, 2 and 3 mL/min, respectively), which leads to the conclusion that a smaller FR potentiates thinner layers. Also, the presence of different colors on thin film images is often associated with thickness non-uniformity throughout the sample and could be caused by thin film malformation, due to low T.

For these reasons, an FR of 0.5 mL/min and 350°C of T (this last one being the reported ideal T for SnS, see section 2.3.1) were chosen to proceed to group G of samples, where deposition time was studied. In these samples, the increase of T seems to help with the uniformity of the layer, but accumulations of material are visible and more intensive with higher t. As no direct conclusions could be drawn about deposition time, 60 seconds, the intermediate value, was used in the next round of samples.

Then, the substrate temperature at deposition was studied, with applied values between 150 and 350°C (sample group H, where sample H5 was done applying the same parameters as sample G2, but on a different day). According to literature, for substrate temperatures higher than 400 °C, SnO is often formed, while for temperatures below 300°C the phases of Sn_2S_3 and SnS_2 are more frequent [52]. It is possible to see that, at lower T, the formed layers seem to be more irregular than the ones deposited at higher T. However, no big differences are verified between 250 and 350°C, where the accumulations of material are still visible.

To improve this, knowing about the influence of the nozzle height on the Oxide X films uniformity, as seen in section 4.2.1, a study of the influence of this parameter was also done for SnS films (Figure 4.7), keeping T at 350 °C, t at 60 s and FR at 0.5 mL/min (sample group I). As verified with the study of Oxide X thin films, increasing the nozzle height results in uniform films without the material accumulations present when H=5 cm, which is also confirmed by the analysis of the films' profiles. When the nozzle is H=11 cm (the highest nozzle height tested), the film's profile shows variations of around 5 nm, without any visible irregularities. Considering this finding, further studies used H of 11 cm as a fixed parameter, to ensure good films' uniformity.

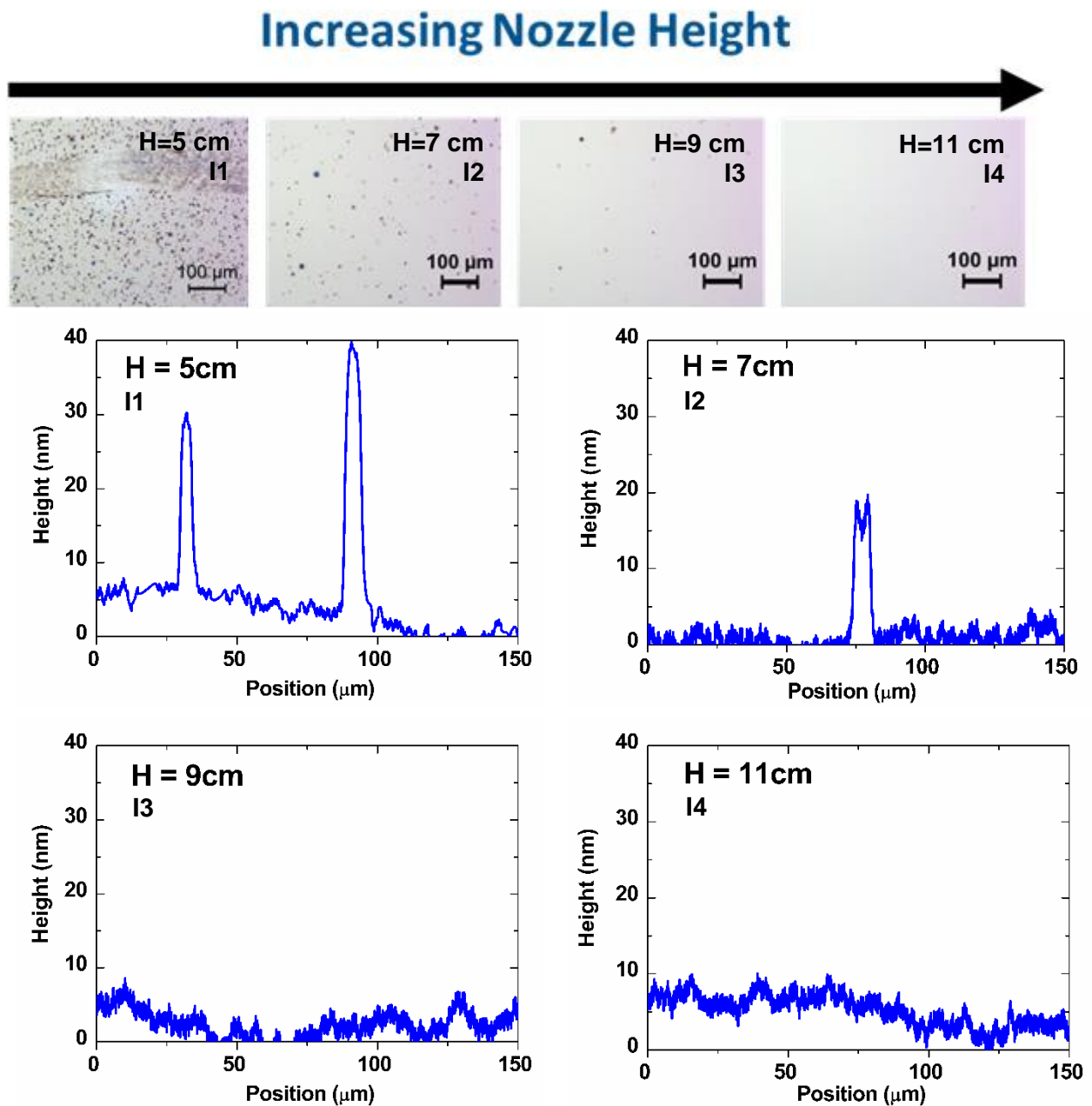


Figure 4.7 – Optical images (on top) and film profiles (on the bottom) of SnS samples deposited using different nozzle heights, of 5, 7, 9 and 11 cm, for samples I1, I2, I3 and I4, respectively.

It can be seen from the SEM images of the samples with films deposited at 300, 350 and 400 °C (while keeping the parameters used for set I of samples constant), that the crystal growth is different (Figure 4.8). Using lower deposition temperatures (300 and 350 °C), cylindrical structures can be observed, possibly because the films growth rate is lower, giving time for these shapes to be formed, while in the film deposited at 400 °C spherical structures are present. This could be an indication that the films are composed of different phases of SnS, meaning that the substrate temperature plays an important role in the characteristics of final layer. This has also been indicated by several different groups [45], [48], [52], [54]. EDS analysis was run to understand if such morphology difference would result in a compositional change, being verified that both tin and sulfur are present in all the samples. The ratio of S/Sn could be obtained through the relative atomic percentages of those elements, being 1:2, 1:1 and 1:5 for temperatures of 300, 350 and 400 °C, respectively. The ratio of 1:1 verified at 350 °C, suggests

a higher chance of achieving the desired tin sulfide phase, SnS, at that temperature, result supported by literature [48], [52].

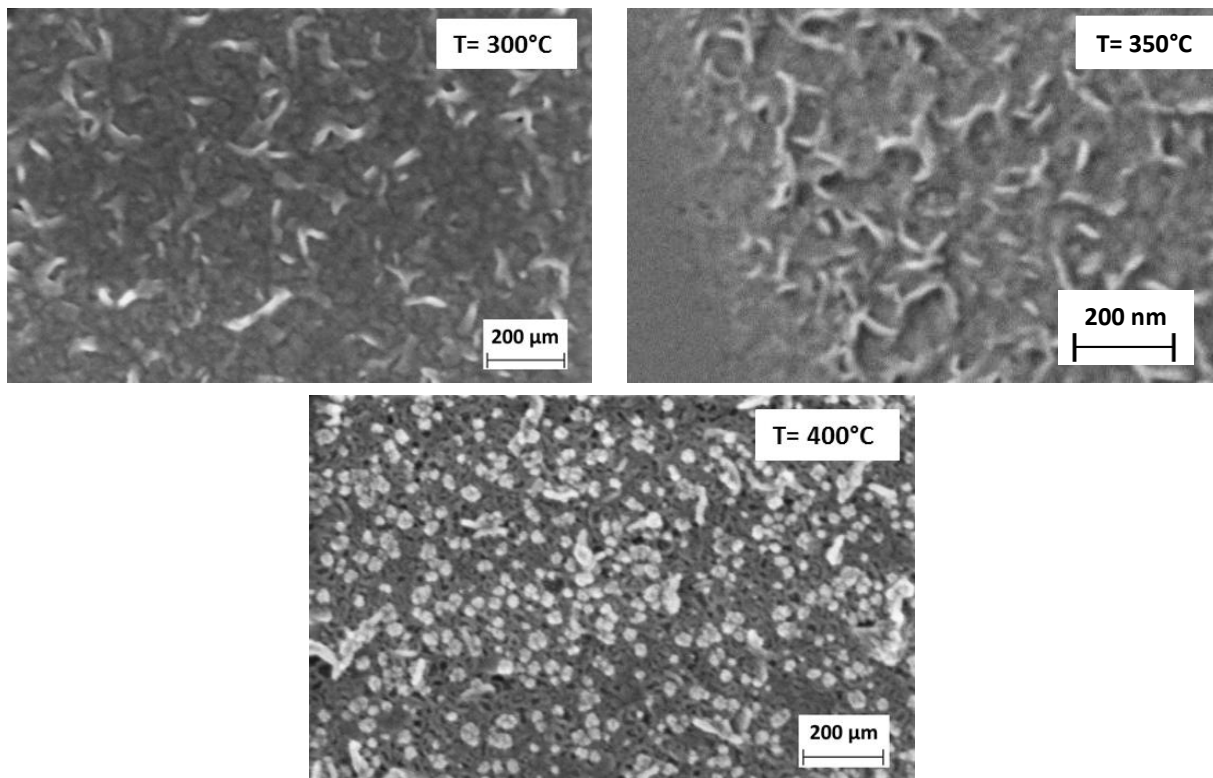


Figure 4.8 - SEM images of the SnS films deposited at T of 300, 350 and 400 °C.

XRD analysis was also performed for further insights into this, but the low thickness of the films did not allow the appropriate signal capture necessary to draw any conclusions, even when using a grazing incidence setup.

4.3.2. TFTs electrical measurements

Considering the results of the SEM/EDS analysis, a temperature influence study was performed by depositing layers using the same conditions used in set I of samples at different temperatures (325, 350, 375 and 400°C), as can be seen in Figure 4.9.

By analyzing these transfer curves, it is possible to conclude that the differences of morphology and composition previously seen in Figure 4.8 influence the materials electrical behavior and hence its conductivity. By increasing the deposition temperature and keeping all the other conditions constant, the TFT show higher drain currents for the same gate voltage sweep. However, the only device that presents a clear modulation between off- and on-states is the one with a SnS layer deposited at 350°C. This could be explained by the study performed by Koteeswara Reddy et al., where higher Hall mobility ($1.4 \text{ cm}^2/(\text{V}\cdot\text{s})$) and carrier densities (10^{17} cm^{-3}) were reported for films deposited at temperatures higher than 400°C and lower values of the same quantities (10^{15} cm^{-3} for carrier density and below $1 \text{ cm}^2/(\text{V}\cdot\text{s})$ for the Hall mobility) for films deposited at temperatures lower than 300°C [48]. Also, Sajeesh et al., using the same salt concentration on their precursor solution, have reported that films deposited at 350°C are of SnS [52], with no other phases present, suggesting that this phase is the most appropriate for proper operation of TFTs. Considering these results and the SEM/EDS characterization previously mentioned, the deposition temperature of 350 °C was used on further sets of experiments.

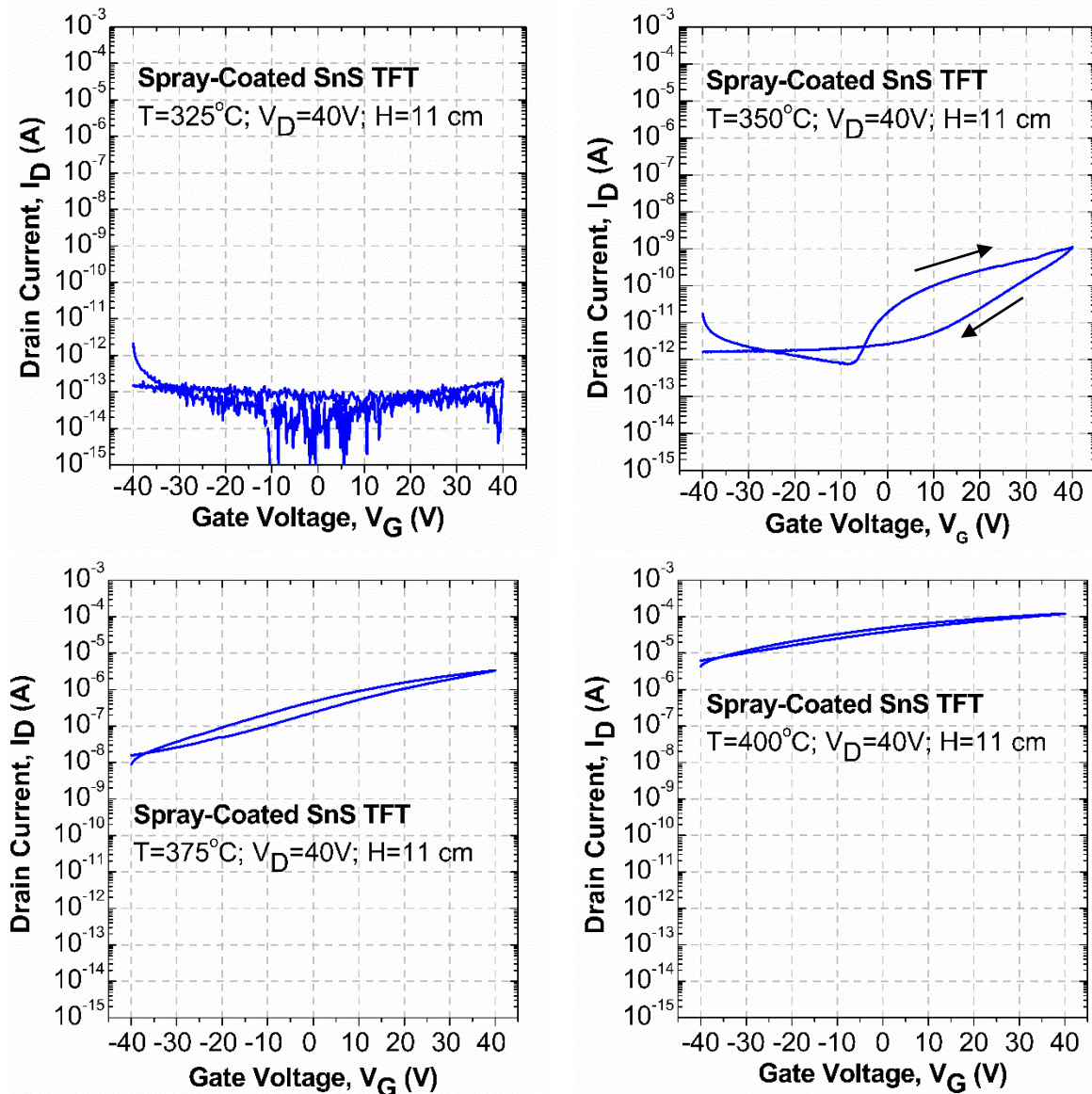


Figure 4.9 – Comparison of the transfer curves of TFTs with SnS semiconductor layers deposited at different substrate temperatures (T). Arrows indicate the V_G sweep direction, showing a clockwise hysteresis.

Transfer characteristics of transistors with different W/L were also made, as seen on Figure 4.10. The respective characteristic parameters values of these three devices can be seen on Table 4.3. Different channel lengths were evaluated, with the scaling of maximum I_D as L decreases being also verified here, as in section 4.2.2 for spin-coated TFTs. In the present case, the I_D increase is more notorious than equation 2.2 would predict (which naturally affects the μ_{SAT} trend). This is related with the V_{ON} shift towards negative values as L decreases, which might be related with the very large electrical resistivity of the SnS layers, providing an easier channel formation for smaller L , as the channel resistance is decreased. When compared to Figure 4.6a (spray-coated oxide X TFTs) this V_{ON} shift is considerably more evident for SnS. While in the case of oxide X TFTs lack of uniformity should justify the apparent random evolution of electrical performance with L , for SnS films deposited under these conditions, the trend with L should be dictated by the total channel resistance, as no coffee-ring effect or other film irregularities were detected.

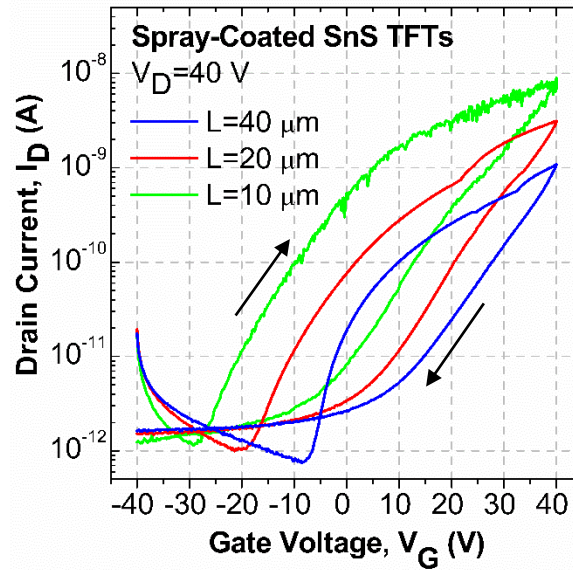


Figure 4.10 – Comparison of transfer curves of spray-coated SnS TFTs with different channel lengths located on the same substrate, with T at 350 °C. Arrows indicate the V_G sweep direction, showing a clockwise hysteresis.

Table 4.3 – Extracted characteristic parameters values from **Figure 4.10** of the produced SnS TFTs, considering different transistor channel lengths.

Channel Length, L (μm)	Saturated Mobility ($\text{cm}^2/(\text{V}\cdot\text{s})$)	V_{ON} (V)	Threshold Voltage, V_T (V)	On/Off Ratio	SS (V/dec)
40	2.8×10^{-6}	-7	4.3×10^{-1}	1.4×10^3	3.5
20	4.6×10^{-6}	-19	3.0×10^{-1}	3.0×10^3	5.8
10	6.7×10^{-6}	-28	-6.9×10^{-2}	9.0×10^3	1.6

Few reports have been made on the study of SnS films applied to electronics as a semiconductor layer. To our knowledge, no SnS based TFT has been reported, turning the results described here quite innovative to the scientific community.

4.3.3. Phototransistor

Considering that the optical band gap of SnS thin films has been reported to be in the order of 1.2 - 1.5 eV, the materials' sensitivity to visible light was to be expected. So, as the TFTs were exposed to light, their electrical response was measured.

When exposed to a yellow light source, the SnS TFTs show a clear off-current increase of about one order of magnitude and V_T shifts towards negative values (Figure 4.11), suggesting charge injection in the semiconductor material. It is visible that the mobility plays an important role in the reaction speed of the TFT, as the one with L of 40 μm (which has a lower mobility) does not return immediately to its initial state. Given more time to recover, the device would present a transfer curve similar to the original one measured. This issue is not observed in the L=10 μm TFT and, therefore, further steps of the study were performed with this device.

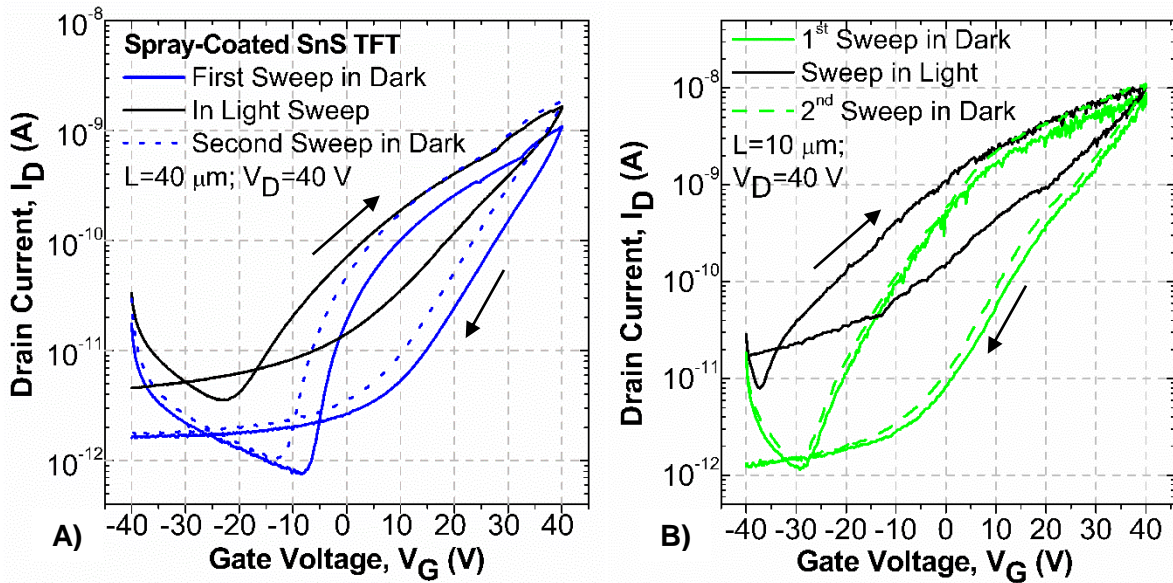


Figure 4.11 - Transfer curves of SnS TFTs before, during and after exposure to a yellow light source. **A)** Transistor with channel length of 40 μm . **B)** Transistor with channel length of 10 μm . Arrows indicate the V_G sweep direction, showing a clockwise hysteresis in both TFTs.

In Figure 4.12 a transient response study is shown for a SnS TFT with $L=10 \mu\text{m}$.

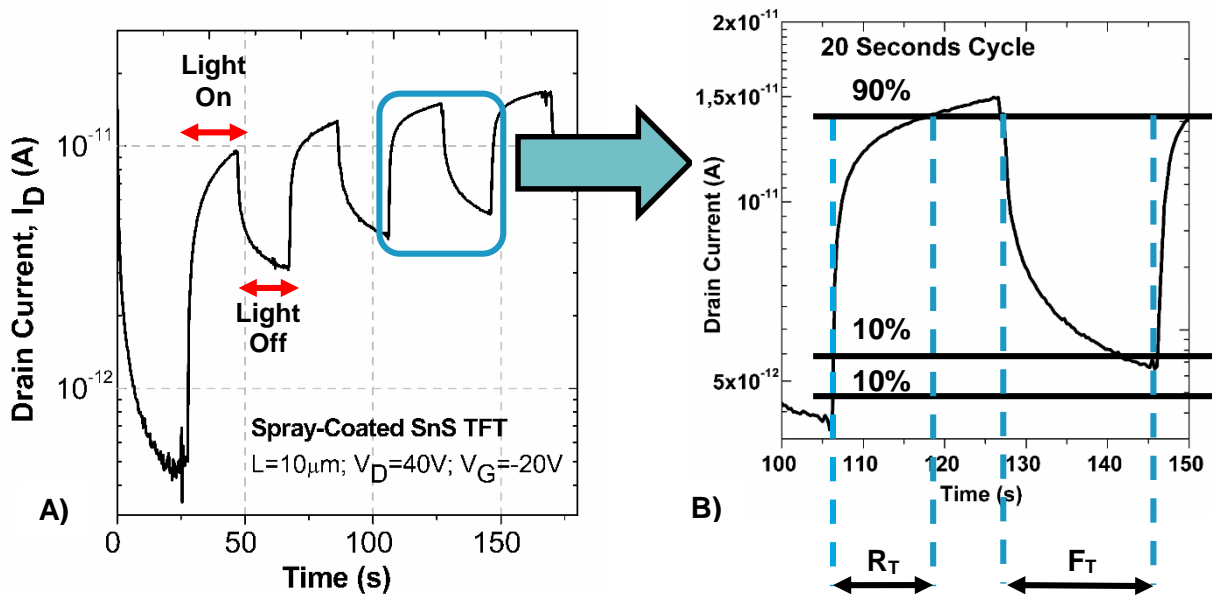


Figure 4.12 - Transient Response of a SnS phototransistor when exposed to light. **A)** Cycles of 20 seconds of light on and off. **B)** Analysis of a single cycle and consequent determination of fall and rise times.

Even though the difference between dark and on current is small, it is possible to see a clear and reproducible response to light cycles of 20 seconds. However, from cycle to cycle the current values increase, suggesting an accumulation of carriers in the conduction band. When analyzing a single cycle, the rise and fall times were calculated, been considered the time between 10% and 90% of the on current, such as described by [78]. These time intervals are in the order of 10 seconds, which is considerably high considering the MoS₂ phototransistor reported values (around 50 ms for an entire cycle, meaning rise and fall time) [79]. However, it should be considered that neither the devices nor the experimental setup reported here are specifically tuned for phototransistor applications. In particular, devices with larger mobilities yield would considerably improve the phototransistor performance.

A final experiment was done on similar SnS TFTs to discard the possibility that the off-current variation

could be attributed to local temperature changes of the devices, while the yellow light was switched on and off. For that end, a similar photoresponse analysis was done using IR radiation, which results in an energy of radiation lower than the SnS bandgap. As can be seen in Figure 4.13 A), devices are insensitive to IR radiation, reinforcing their operation as phototransistors with visible light wavelengths.

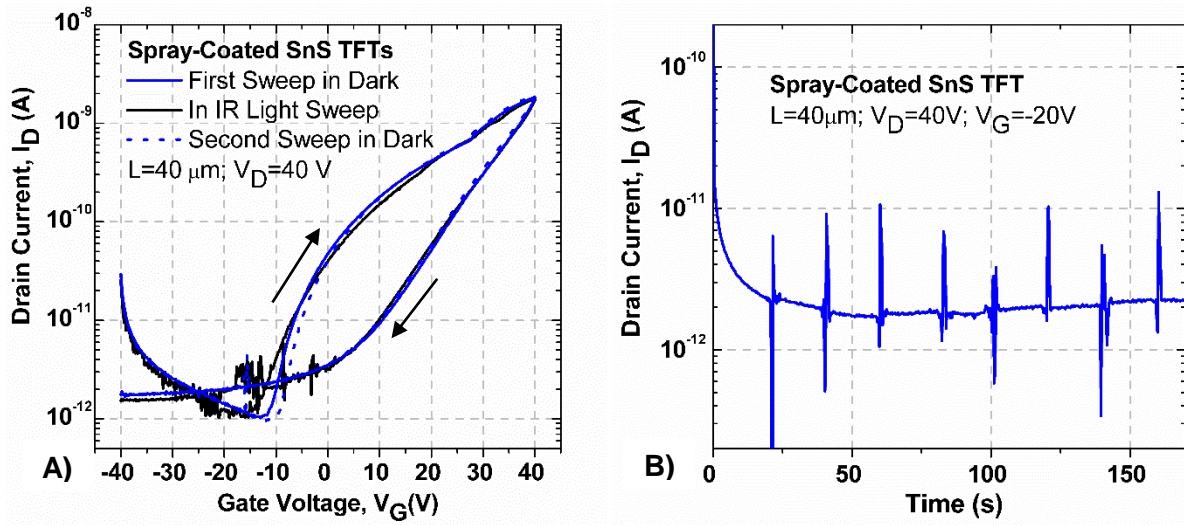


Figure 4.13 - Response of Spray-Coated TFTs to Infrared Light. **A)** Transfer curves of a TFT with $L=40 \mu\text{m}$ before, during and after IR light exposure. Arrows indicate the V_G sweep direction, showing a clockwise hysteresis. **B)** Transient response of the same TFT to IR light.

5. CONCLUSIONS

In this research a spray coating deposition system was implemented and studied, as a low cost and easily applicable technique for producing functional TFTs, using different semiconductor materials, such as oxides and chalcogenides. The system's potential for industrial applications was explored, aiming for the assessment of its versatility and easiness to work with. This project was done for TNO in Holst Centre, as part of an internship. Within Holst Centre, the CSC method was relatively unexplored, so it was necessary to setup the system, test it and optimize it to ensure it was working properly and that it could deposit suitable thin films. The evolution of the project was solely based on the conclusions drawn on small steps taken and on the available literature, as the group had limited experience with the technique.

Firstly, ZnO was tested as a standard semiconductor material, due to its usage in previous work done by another research group within the organization and to the availability of studies on spray-coated ZnO based TFTs. Even though all the steps of the process (precursor solution choice, parameters employed, substrates used) were based on the literature, this step of the project was still challenging, since an adaptation to the implemented system had to be done. Solution flow-rate and deposition time influences were tested, reaching an optimal set of parameters for this material. While keeping the solution flow-rate constant, a linear relation between film thickness and time was achieved and uniform films with roughness below 5 nm were obtained. Applying the same layers into transistor substrates resulted in TFTs with unpatterned ZnO layers, presenting mobilities of $0.14 \text{ cm}^2/(\text{V}\cdot\text{s})$ and on/off ratios up to 10^6 .

Then, a commercial solution initially optimized for spin-coating to produce Oxide X films was applied with CSC, using low substrate temperatures of 40°C to closely mimic spin-coating conditions. The testing of the CSC technique for adaptability was the aim of this experiment, as it was an easy way of comparing two low-cost techniques, spin-coating and spray-coating. Some experiments were initially made to reach uniform films, as the influence of most of the deposition parameters was studied, always trying to keep substrate temperature below 100°C and setting the air-pressure to 1 bar. The nozzle height turned out to be an important parameter, as heights of 9 and 11 cm seemed to produce very uniform films, while at 5 and 7 cm the films presented accumulations of material. These irregularities could be seen at an optical microscope level in transistor substrates, as opposed to the spin-coated substrates, where the film was much more uniform. These differences in morphology caused by the slow evaporation of solvent that happens due to the application of low-substrate temperatures could explain the $10^3 \text{ cm}^2/(\text{V}\cdot\text{s})$ higher mobilities in spin-coated, as coffee-ring shaped irregularities in the films processed by CSC were obtained.

Finally, SnS application as a semiconductor in TFTs was explored. As chalcogenides have attracted interest lately due to their expected high mobilities and since SnS was still relatively unexplored, studying this material presented the opportunity of confirming the CSC versatility. Also, SnS had been reported to be photosensitive, which allowed the study of its photodetection capabilities as a final goal. Due to the lack of reports of SnS film with nanometer thickness, a broad study of the initial conditions had to be done with this material. Starting with the precursor solution choice, where a study of the best solvent had to be made, the substrate temperature was also varied, being found it influences the conductivity of the film. Lastly, similarly to the Oxide X study, the nozzle height was found to have a determinant effect on the film's uniformity. TFTs done with the optimized films presented low mobilities, in the magnitude of $10^{-6} \text{ cm}^2/(\text{V}\cdot\text{s})$, but successfully worked as switches. On the other hand, when exposed to light the devices worked as phototransistors, showing a clear and reversible response to yellow visible light, reflected in a drain-to-source current variation of several cycles. To the author's knowledge, this was the first report of SnS TFTs in literature.

As the semiconductor industry searches for simple, but effective ways of depositing thin films, solution based methods have attracted the researchers' interest in the past few years. Also, the chalcogenide group of semiconductor materials, with the promise of high mobilities and good device performance, have been explored for applications where graphene cannot be used, such as digital electronics and switching. In this work, both were combined together, producing a base ground for future research in the field.

6. FUTURE PERSPECTIVES

Even though relevant conclusions can be drawn from the experiments performed, some improvements can be done to the process used. Also, supporting tests can be performed to further complement the obtained results and to take the project to the next level. In this section, some suggestions and future perspectives are presented.

While the unpatterned semiconductor TFT model was ideal for the initial tests, in an advanced study the development of a masking procedure is advisable, as the devices produced would have closer behavior to what is aimed for in the industry. Also, a study of the best dielectric and electrodes for each specific semiconductor layer could be done, to help improve the device functionality.

Regarding the Oxide X comparative study between spin-coating and spray-coating, it is believed that a new experiment employing higher substrate temperature during CSC should be tried. The use of temperature could prevent the formation of the structures obtained at ambient temperature deposition, resulting in more uniform films, without coffee-ring structures being formed. On the other hand, since the precursor solution for Oxide X has been previously optimized for spin-coating, modifications on it could also contribute to improvements, such as using a more appropriate solvent for CSC.

Concerning the SnS films, it is believed that a deeper initial study of the precursor solution composition is required, since in this project we based our salt, molarity and solvent choice on the available literature reports, as the focus was the final application. This could significantly help increase the thin film's quality, which would directly affect the phototransistor characteristics and parameters. One new approach could be the use of a single SnS precursor, such as the one synthesized by K. Ramasamy et al. [80]. Although it might increase the final cost of the process, the use of a single precursor could avoid some of the problems associated with two-precursor solutions, such as phase segregation that happens when the precursors present different solubilities [3]. On the other hand, once a transistor with enhanced working characteristics is optimized, a deeper study of the devices responsivity to light could be performed, including variations of light wavelength, intensity of irradiation (power) and dynamic response (applying cycles of different time intervals and checking the devices' speed).

Ultimately, the presented work corresponds to the initial steps of a long-term project, as further steps can be taken on the optimization of the CSC process to application in industrial environment. Other materials can be tested and other devices could be made with those layers, as proof of concept.

Also, the study of chalcogenides for application in electronics has been focused on in the past few years, as the need for an alternative to silicon increases. Even though these materials were among the first semiconductors to be tested for transistor application, the high mobilities they can reach have raised a new interest in them throughout the scientific community. Therefore, there is much room and benefit in performing further studies on these materials.

REFERENCES

- [1] A. Munjer, H. Rahman Habib, and A. Raihan, "Chapter III: Experimental," in *Thin Film Deposition by Spray Pyrolysis Technique: Automatic Control of Spray Pyrolysis, Film Characterization, Application in Solar Cell*, LAMBERT Academic Publishing, 2012, pp. 39 – 54.
- [2] J. S. Skarman and R. R. Chamberlin, "Chemical Spray Deposition Process for Inorganic Films," *J. Electrochem. Soc.*, vol. 113, no. 1, pp. 86–89, 1966.
- [3] A. Gurav, T. Kodas, T. Pluym, and Y. Xiong, "Aerosol Processing of Materials," *Aerosol Sci. Technol.*, vol. 19, no. 4, pp. 411–452, Jan. 1993.
- [4] P. S. Patil, "Versatility of chemical spray pyrolysis technique," *Mater. Chem. Phys.*, vol. 59, no. 3, pp. 185–198, Jun. 1999.
- [5] D. Perednis and L. J. Gauckler, "Thin Film Deposition Using Spray Pyrolysis," *J. Electroceramics*, vol. 14, no. 2, pp. 103–111, Mar. 2005.
- [6] S. M. Sabnis, P. A. Bhadane, and P. G. Kulkarni, "Process flow of spray pyrolysis technique," *J. Appl. Phys.*, vol. 4, no. 5, pp. 7–11, 2013.
- [7] N. Sahu, B. Parija, and S. Panigrahi, "Fundamental understanding and modeling of spin coating process: A review," *Indian J. Phys.*, vol. 83, no. 4, pp. 493–502, Aug. 2009.
- [8] Ossila, "Spin Coating: A Guide to Theory and Techniques." [Online]. Available: <http://www.ossila.com/pages/spin-coating>. [Accessed: 20-Sep-2015].
- [9] D. B. Mitzi, L. L. Kosbar, C. E. Murray, M. Copel, and A. Afzali, "High-mobility ultrathin semiconducting films prepared by spin coating," *Nature*, vol. 428, no. 18 March 2004, pp. 299–303, 2004.
- [10] A. L. Dawar and J. C. Joshi, "Semiconducting transparent thin films: their properties and applications," *J. Mater. Sci.*, vol. 19, no. 1, pp. 1–23, 1984.
- [11] J. F. Wager, D. A. Keszler, and R. E. Presley, *Transparent Electronics*. Boston, MA: Springer US, 2008, pp. 1–8.
- [12] H. Morkoç and U. Ozgur, *Zinc Oxide: Fundamentals, Materials and Device Technology*. Wiley-VCH, 2009.
- [13] C. F. Klingshirm, B. K. Meyer, A. Waag, A. Hoffmann, and J. Geurts, *Zinc Oxide: From Fundamentals Properties Towards Novel Applications*. Springer, 2010.
- [14] O. D. Applications, *Zinc Oxide Materials for Electronic and Optoelectronic Device Applications*. Chichester, UK: John Wiley & Sons, Ltd, 2011.
- [15] C. Jagadish and S. Pearton, *Zinc Oxide Bulk, Thin Films and Nanostructures*, 1st ed. Elsevier, 2006.
- [16] E. Terukov and N. H. Nickel, Eds., *Zinc Oxide - A Material for Micro- and Optoelectronic Application*. 2005.
- [17] E. R. Hull, J. Parisi, and P. C. Fibers, *Transparent Conductive Zinc Oxide: Basic and Applications in Thin Film Solar Cells*. Springer, 2008.

- [18] Z. Chuan, *Handbook of Zinc Oxide and Related Materials Volume Two Devices and Nano-Engineering*. CRC Press, 2013.
- [19] S. Pearton, *GaN and ZnO-based Materials and Devices*. Springer, 2012.
- [20] U. Özgür, Y. I. Alivov, C. Liu, a. Teke, M. a. Reshchikov, S. Doğan, V. Avrutin, S.-J. Cho, and H. Morkoç, "A comprehensive review of ZnO materials and devices," *J. Appl. Phys.*, vol. 98, no. 4, p. 041301, 2005.
- [21] E. Fortunato, a. Pimentel, L. Pereira, a. Gonçalves, G. Lavareda, H. Águas, I. Ferreira, C. N. Carvalho, and R. Martins, "High field-effect mobility zinc oxide thin film transistors produced at room temperature," *J. Non. Cryst. Solids*, vol. 338–340, pp. 806–809, Jun. 2004.
- [22] J. Kim, J. Meng, D. Lee, M. Yu, D. Yoo, D. W. Kang, and J. Jo, "ZnO Thin-Film Transistor Grown by rf Sputtering Using Carbon Dioxide and Substrate Bias Modulation," *J. Nanomater.*, vol. 2014, pp. 1–7, 2014.
- [23] P. F. Carcia, R. S. McLean, M. H. Reilly, and G. Nunes, "Transparent ZnO thin-film transistor fabricated by rf magnetron sputtering," *Appl. Phys. Lett.*, vol. 82, no. 7, p. 1117, 2003.
- [24] G. Kaur, A. Mitra, and K. L. Yadav, "Pulsed laser deposited Al-doped ZnO thin films for optical applications," *Prog. Nat. Sci. Mater. Int.*, vol. 25, no. 1, pp. 12–21, Feb. 2015.
- [25] E. Fazio, S. Patanè, S. Scibilia, a. M. Mezzasalma, G. Mondio, F. Neri, and S. Trusso, "Structural and optical properties of pulsed laser deposited ZnO thin films," *Curr. Appl. Phys.*, vol. 13, no. 4, pp. 710–716, Jun. 2013.
- [26] M. G. Tsoutsouva, C. N. Panagopoulos, D. Papadimitriou, I. Fasaki, and M. Kompitsas, "ZnO thin films prepared by pulsed laser deposition," *Mater. Sci. Eng. B*, vol. 176, no. 6, pp. 480–483, Apr. 2011.
- [27] A. J. Petrella, H. Deng, N. K. Roberts, and R. N. Lamb, "Single-Source Chemical Vapor Deposition Growth of ZnO Thin Films Using Zn 4 O (CO 2 NEt 2) 6," *Chem. Mater.*, vol. 85, no. 5, pp. 4339–4342, 2002.
- [28] J. G. Lu, T. Kawaharamura, H. Nishinaka, Y. Kamada, T. Ohshima, and S. Fujita, "Zno-based thin films synthesized by atmospheric pressure mist chemical vapor deposition," *J. Cryst. Growth*, vol. 299, no. 1, pp. 1–10, Feb. 2007.
- [29] K. Shum, T. Salagaj, and K. Strobl, "ZnO thin films synthesized by chemical vapor deposition," *2010 IEEE Long Isl. Syst. Appl. Technol. Conf.*, pp. 1–6, 2010.
- [30] N. V Kaneva and C. D. Dushkin, "Preparation of nanocrystalline thin films of ZnO by sol-gel dip coating," *Bulg. Chem. Commun.*, vol. 43, no. 2, pp. 259–263, 2011.
- [31] K. Thongsuriwong, P. Amornpitoksuk, and S. Suwanboon, "Structure, morphology, photocatalytic and antibacterial activities of ZnO thin films prepared by sol-gel dip-coating method," *Adv. Powder Technol.*, vol. 24, no. 1, pp. 275–280, Jan. 2013.
- [32] M. Smirnov, C. Baban, and G. I. Rusu, "Structural and optical characteristics of spin-coated ZnO thin films," *Appl. Surf. Sci.*, vol. 256, no. 8, pp. 2405–2408, Feb. 2010.
- [33] O. Singh, N. Kohli, M. P. Singh, K. Anand, and R. C. Singh, "Gas sensing properties of zinc oxide thin films prepared by spray pyrolysis," in *Gas sensing properties of zinc oxide thin films prepared by spray pyrolysis*, 2012, vol. 191, no. 1, pp. 191–193.

- [34] A. Bashir, P. H. Wöbkenberg, J. Smith, J. M. Ball, G. Adamopoulos, D. D. C. Bradley, and T. D. Anthopoulos, "High-Performance Zinc Oxide Transistors and Circuits Fabricated by Spray Pyrolysis in Ambient Atmosphere," *Adv. Mater.*, vol. 21, no. 21, pp. 2226–2231, Jun. 2009.
- [35] E. Fortunato, P. Barquinha, a. Pimentel, a. Gonçalves, a. Marques, L. Pereira, and R. Martins, "Recent advances in ZnO transparent thin film transistors," *Thin Solid Films*, vol. 487, no. 1–2, pp. 205–211, Sep. 2005.
- [36] Y. Jeong, C. Pearson, Y. U. Lee, L. Winchester, J. Hwang, H. Kim, L.-M. Do, and M. C. Petty, "Zinc Oxide Thin-Film Transistors Fabricated at Low Temperature by Chemical Spray Pyrolysis," *J. Electron. Mater.*, vol. 43, no. 11, pp. 4241–4245, Aug. 2014.
- [37] W. Ren and H.-M. Cheng, "The global growth of graphene.," *Nat. Nanotechnol.*, vol. 9, no. 10, pp. 726–730, Oct. 2014.
- [38] D. Jariwala, V. K. Sangwan, L. J. Lauhon, T. J. Marks, and M. C. Hersam, "Emerging device applications for semiconducting two-dimensional transition metal dichalcogenides.," *ACS Nano*, vol. 8, no. 2, pp. 1102–20, Feb. 2014.
- [39] A. Qurashi, Ed., *Metal Chalcogenide Nanostructures for Renewable Energy*. Scrivener Publishing LLC., 2015.
- [40] R. Scheer and H.-W. Schock, *Chalcogenide Photovoltaics*. Weinheim, Germany: Wiley-VCH Verlag GmbH & Co. KGaA, 2011.
- [41] B. Radisavljevic, A. Radenovic, J. Brivio, V. Giacometti, and A. Kis, "Single-layer MoS₂ transistors," *Nat. Nanotechnol.*, vol. 6, pp. 147–150, 2011.
- [42] A. Carrillo-Castillo, A. Salas-Villasenor, I. Mejia, S. Aguirre-Tostado, B. E. Gnade, and M. a. Quevedo-López, "P-type thin films transistors with solution-deposited lead sulfide films as semiconductor," *Thin Solid Films*, vol. 520, no. 7, pp. 3107–3110, Jan. 2012.
- [43] K. T. R. Reddy, N. K. Reddy, and R. W. Miles, "Photovoltaic properties of SnS based solar cells," *Sol. Energy Mater. Sol. Cells*, vol. 90, no. 18–19, pp. 3041–3046, 2006.
- [44] D. Avallaneda, G. Delgado, M. T. S. Nair, and P. K. Nair, "Proceedings of Symposium O on Thin Film Chalcogenide Photovoltaic Materials, EMRS 2006 Conference EMRS 2006 Symposium O," *Thin Solid Films*, vol. 515, no. 15, pp. 5745–6288, 2007.
- [45] M. Calixto-Rodriguez, H. Martinez, A. Sanchez-Juarez, J. Campos-Alvarez, A. Tiburcio-Silver, and M. E. Calixto, "Structural, optical, and electrical properties of tin sulfide thin films grown by spray pyrolysis," *Thin Solid Films*, vol. 517, no. 7, pp. 2497–2499, Feb. 2009.
- [46] P. Sinsersuksakul, K. Hartman, S. Bok Kim, J. Heo, L. Sun, H. Hejin Park, R. Chakraborty, T. Buonassisi, and R. G. Gordon, "Enhancing the efficiency of SnS solar cells via band-offset engineering with a zinc oxysulfide buffer layer," *Appl. Phys. Lett.*, vol. 102, no. 5, p. 053901, 2013.
- [47] V. Steinmann, R. Jaramillo, K. Hartman, R. Chakraborty, R. E. Brandt, J. R. Poindexter, Y. S. Lee, L. Sun, A. Polizzotti, H. H. Park, R. G. Gordon, and T. Buonassisi, "3.88% efficient tin sulfide solar cells using congruent thermal evaporation.," *Adv. Mater.*, vol. 26, no. 44, pp. 7488–92, Dec. 2014.
- [48] N. Koteeswara Reddy and K. T. Ramakrishna Reddy, "Electrical properties of spray pyrolytic tin sulfide films," *Solid. State. Electron.*, vol. 49, no. 6, pp. 902–906, Jun. 2005.

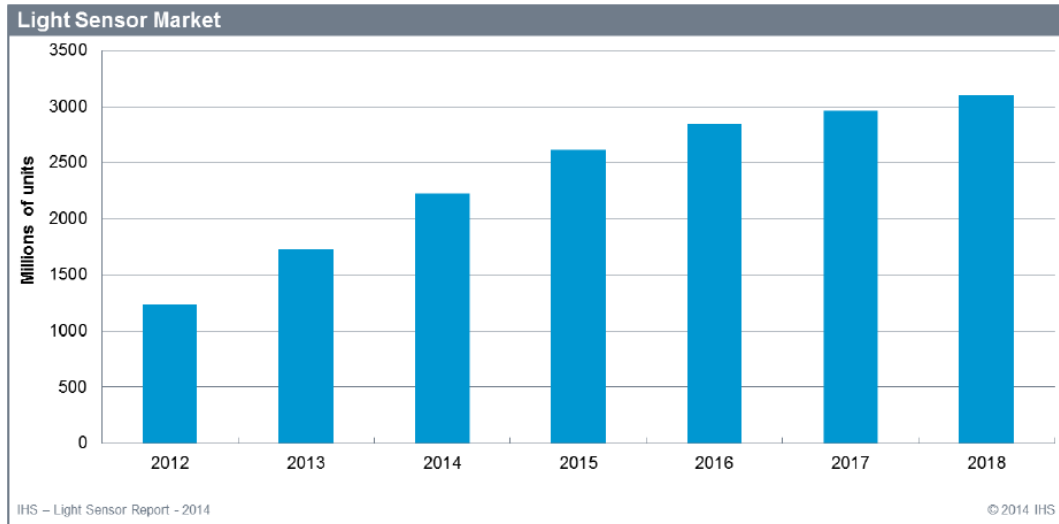
- [49] A. Sanchez-Juarez and A. Ortíz, "Effects of precursor concentration on the optical and electrical properties of SnXSY thin films prepared by plasma-enhanced chemical vapour deposition," *Semicond. Sci. Technol.*, vol. 17, no. 9, pp. 931–937, 2002.
- [50] N. K. Reddy, K. T. R. Reddy, G. Fisher, R. Best, and P. K. Dutta, "The structural behaviour of layers of SnS grown by spray pyrolysis," *J. Phys. D. Appl. Phys.*, vol. 32, no. 9, pp. 988–990, May 1999.
- [51] N. K. Reddy and K. T. R. Reddy, "Optical behaviour of sprayed tin sulphide thin films," *Mater. Res. Bull.*, vol. 41, no. 2, pp. 414–422, Feb. 2006.
- [52] T. H. Sajeesh, A. R. Warriar, C. S. Kartha, and K. P. Vijayakumar, "Optimization of parameters of chemical spray pyrolysis technique to get n and p-type layers of SnS," *Thin Solid Films*, vol. 518, no. 15, pp. 4370–4374, May 2010.
- [53] S. S. Hegde, A. G. Kunjomana, K. Ramesh, K. A. Chandrasekharan, and M. Prashantha, "Preparation and Characterization of SnS Thin Films for Solar Cell Application," *Int. J. Soft Comput. Eng.*, vol. 1, no. NCRAMT2011, pp. 38–40, 2011.
- [54] S. Polivtseva, I. O. Acik, A. Katerski, A. Mere, V. Mikli, and M. Krunks, "Spray Pyrolysis Deposition of SnxSy Thin Films," *Energy Procedia*, vol. 60, pp. 156–165, 2014.
- [55] P. D. Antunez, D. A. Torelli, F. Yang, F. A. Rabu, N. S. Lewis, and R. L. Brutchey, "Low Temperature Solution-Phase Deposition of SnS Thin Films," *Chem. Mater.*, vol. 26, pp. 5444–5446, 2014.
- [56] U. Zschieschang, T. Holzmann, B. V. Lotsch, and H. Klauk, "Tin Disulfide (SnS₂) Thin-Film Field-Effect Transistors," 2014, vol. 23, no. 1990, pp. 267–268.
- [57] D. De, J. Manongdo, S. See, V. Zhang, A. Guloy, and H. Peng, "High on/off ratio field effect transistors based on exfoliated crystalline SnS₂ nano-membranes.," *Nanotechnology*, vol. 24, no. 025202, Jan. 2013.
- [58] Y. Huang, E. Sutter, J. T. Sadowski, M. Cotlet, O. L. a Monti, D. a Racke, M. R. Neupane, D. Wickramaratne, R. K. Lake, B. a Parkinson, and P. Sutter, "Tin disulfide-an emerging layered metal dichalcogenide semiconductor: materials properties and device characteristics," *ACS Nano*, vol. 8, no. 10, pp. 10743–55, Oct. 2014.
- [59] H. S. Song, S. L. Li, L. Gao, Y. Xu, K. Ueno, J. Tang, Y. B. Cheng, and K. Tsukagoshi, "High-performance top-gated monolayer SnS₂ field-effect transistors and their integrated logic circuits," *Nanoscale*, vol. 5, no. 20, p. 9666, 2013.
- [60] U. Zschieschang, T. Holzmann, A. Kuhn, M. Aghamohammadi, B. V. Lotsch, and H. Klauk, "Threshold-voltage control and enhancement-mode characteristics in multilayer tin disulfide field-effect transistors by gate-oxide passivation with an alkylphosphonic acid self-assembled monolayer," *J. Appl. Phys.*, vol. 117, no. 10, p. 104509, Mar. 2015.
- [61] C. K. Kagan and P. Andry, Eds., *Thin-Film Transistors*. CRC Press, 2003.
- [62] S. D. Brotherton, *Introduction to Thin Film Transistors*. Heidelberg: Springer International Publishing, 2013.
- [63] P. Barquinha, "Transparent Oxide Thin-Film Transistors: Production, Characterization and Integration," Universidade Nova de Lisboa, 2010.
- [64] L. Pereira, "Produção e caracterização de silício policristalino e sua aplicação a TFTs," Universidade Nova de Lisboa, 2008.

- [65] D. K. Schroder, *Semiconductor material and device characterization*, 3rd ed. John Wiley & Sons, Ltd, 2006.
- [66] E. Gates, "Semiconductor Devices," in *Introduction to Electronics*, Sixth., Cengage Learning, 2011, pp. 261–265.
- [67] B. Lojek, *History of Semiconductor Engineering*. Springer, 2007, p. 35.
- [68] D. L. J. Morton and J. Gabriel, *Electronics: The Life Story of a Technology*. John Hopkins Paperback, 2007, pp. 45–46.
- [69] C. W. Litton, T. C. Collins, and D. C. Reynolds, *Zinc Oxide Materials for Electronic and Optoelectronic Device Applications*. Wiley, 2011, p. 315.
- [70] R. M. Marston, *Optoelectronics Circuits Manual*. Reed International Book, 1988, pp. 8–9.
- [71] M. Boustany, "Light Sensors Report - 2015," 2015.
- [72] J. Webster and H. Eren, *Measurement, Instrumentation, and Sensors Handbook*, 2nd ed. CRC Press, 2014, pp. 44–7 – 44–8.
- [73] A.-M. Andringa, J. R. Meijboom, E. C. P. Smits, S. G. J. Mathijssen, P. W. M. Blom, and D. M. de Leeuw, "Gate-Bias Controlled Charge Trapping as a Mechanism for NO₂ Detection with Field-Effect Transistors," *Adv. Funct. Mater.*, vol. 21, no. 1, pp. 100–107, Jan. 2011.
- [74] K. Okamura, D. Nikolova, N. Mechau, and H. Hahn, "Appropriate choice of channel ratio in thin-film transistors for the exact determination of field-effect mobility," *Appl. Phys. Lett.*, vol. 94, no. 18, p. 183503, 2009.
- [75] D. Hong, G. Yerubandi, H. Q. Chiang, M. C. Spiegelberg, and J. F. Wager, "Electrical Modeling of Thin-Film Transistors," *Crit. Rev. Solid State Mater. Sci.*, vol. 33, no. 2, pp. 101–132, May 2008.
- [76] H. Frenzel, A. Lajn, and M. Grundmann, "One decade of fully transparent oxide thin-film transistors: fabrication, performance and stability," *Phys. status solidi - Rapid Res. Lett.*, vol. 7, no. 9, pp. 605–615, Sep. 2013.
- [77] E. Fortunato, P. Barquinha, and R. Martins, "Oxide semiconductor thin-film transistors: a review of recent advances," *Adv. Mater.*, vol. 24, no. 22, pp. 2945–2986, 2012.
- [78] V. N. Tran, R. Stuart, and H. Bhavsar, "Phototransistor Switching Time Analysis," *California Eastern Laboratories*. [Online]. Available: <http://www.cel.com/pdf/apnotes/an3009.pdf>.
- [79] Z. Yin, H. Li, H. Li, L. Jiang, Y. Shi, Y. Sun, G. Lu, Q. Zhang, X. Chen, and H. Zhang, "Single-Layer MoS₂ Phototransistors," *ACS Nano*, vol. 6, no. 1, pp. 74–80, 2012.
- [80] K. Ramasamy, V. L. Kuznetsov, K. Gopal, M. A. Malik, J. Raftery, P. P. Edwards, and P. O. Brien, "Organotin Dithiocarbamates: Single-Source Precursors for Tin Sul fi de Thin Films by Aerosol-Assisted Chemical Vapor Deposition (AACVD)," *Chem. Mater.*, vol. 25, pp. 266–276, 2013.

7. ANNEXES

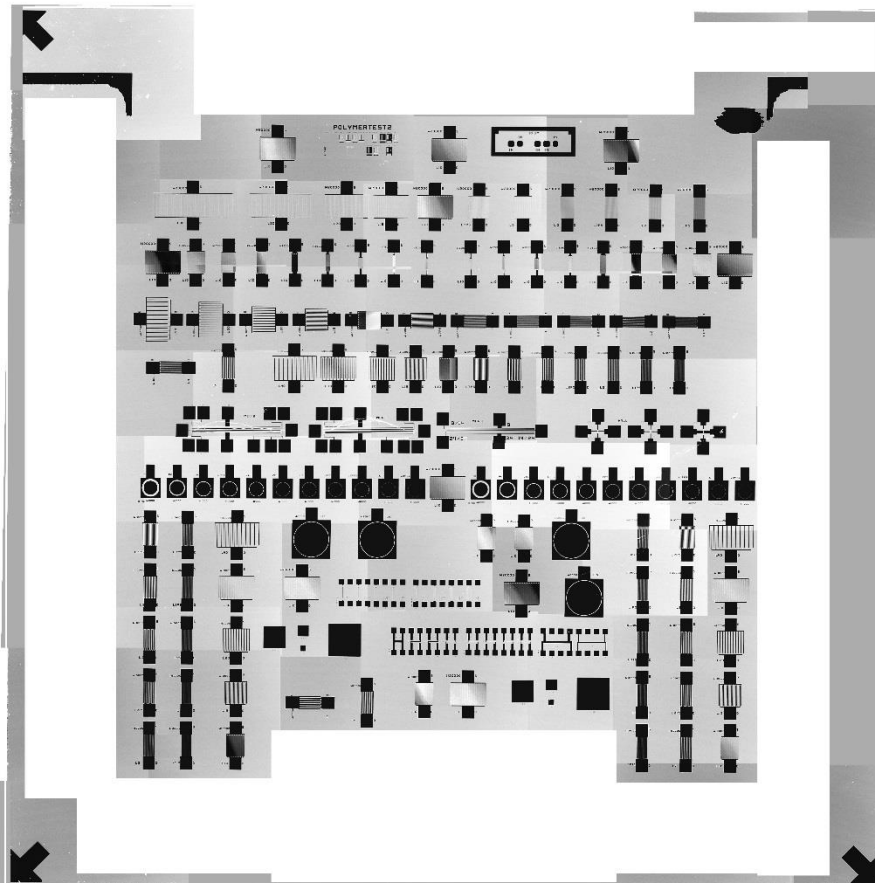
Annex A - Prediction of the market demand for light sensors, where phototransistors can be incorporated, showing an increasing demand over the next few years.

Predictions are made by Marwan Boustany, an IHS analyst, in 2014 [71].



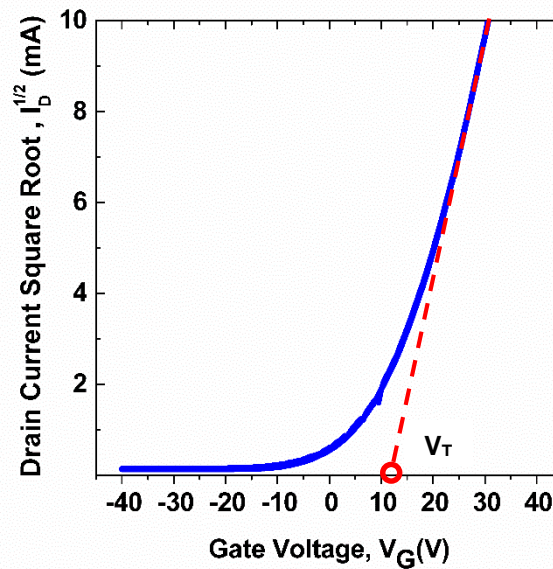
Annex B – Alignment mask used for the contacts of the transistor substrates, where the different transistor layouts can be seen.

Ring transistors (marked above) were chosen to be tested.



Annex C - Extraction method used for obtaining the characteristic parameters of the studied TFTs.

An extrapolation of the linear area of the curve is made to the x-axis, from which is taken the equation of the straight line ($y = mx + b$, where m is the slope and b is the value of intersection with the y-axis). The intersection of this line with the x-axis corresponds to the V_T value (indicated in the circle). The saturated mobility is determined considering the extracted slope m using equation [7.1]. Both values are deduced from equation [2.2], which describes the behaviour of a TFT device working in the saturation region.

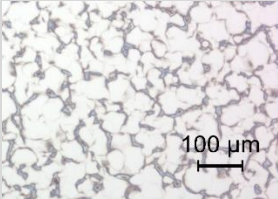
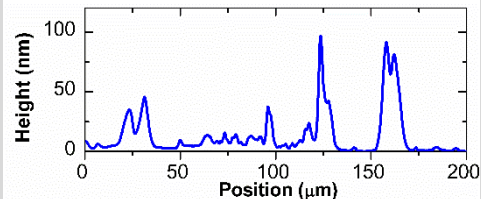
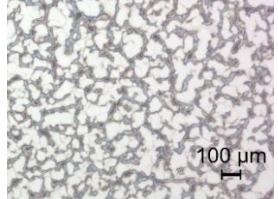
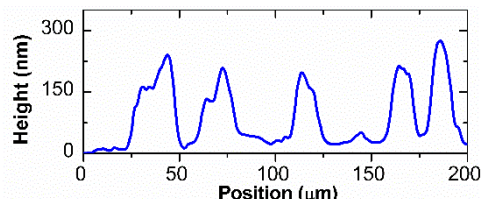
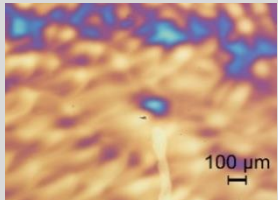
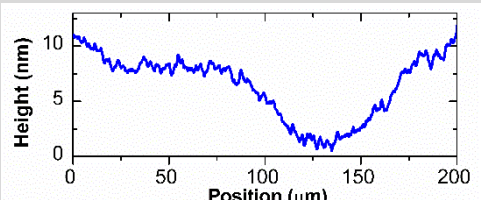
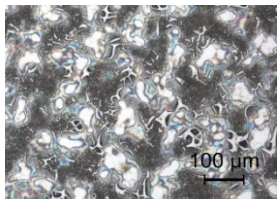
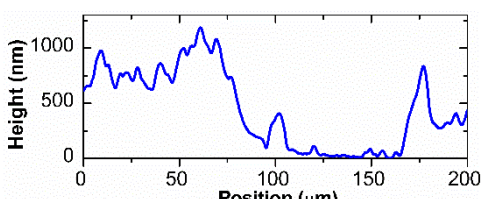


$$\mu_{sat} = \frac{2Lm^2}{WC_i} \quad [7.1]$$

Spray Coating of Oxide and Chalcogenide Semiconductor Layers for TFT Application

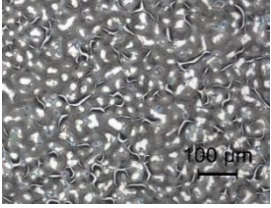
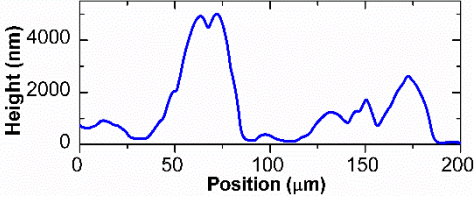

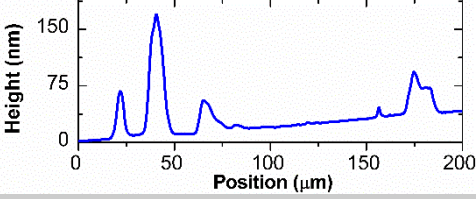
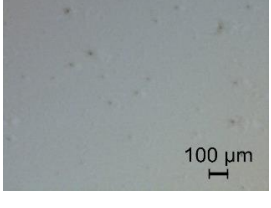
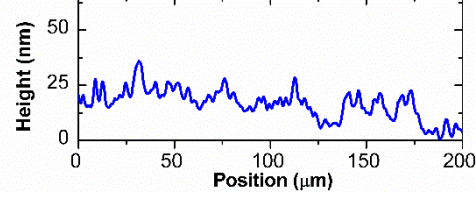
Annex D – Deposition parameters used for spray coating deposition of different samples of oxide X thin films and respective optical images and film profiles.

T – substrate temperature during deposition; FR – Flow-Rate of solution; t – Deposition time; H – distance between nozzle and substrate.

Sample	Precursor Solution	T (°C)	FR (mL/min)	t (s)	H (cm)	Optical Images	Film Profiles
A1	Original	40	0.1	15	5		
A2	Original	40	0.1	30	5		
B1	Original	40	0.5	30	5		
B2	Original	60	0.5	30	5		

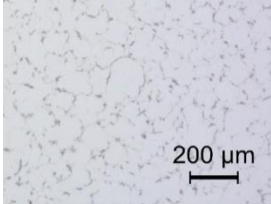
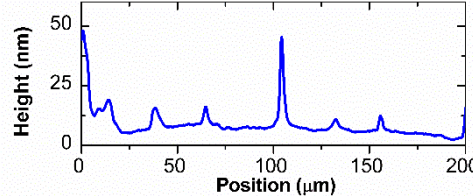
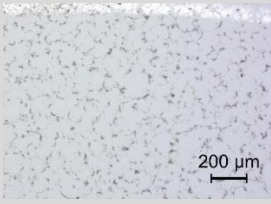
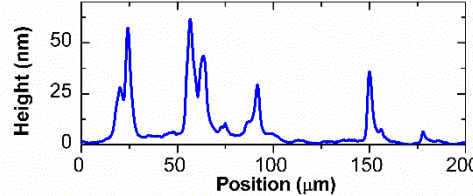
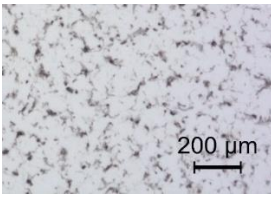
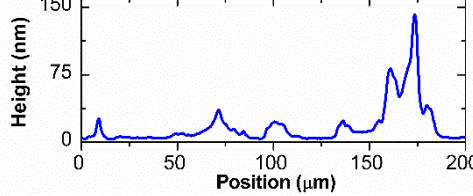
Spray Coating of Oxide and Chalcogenide Semiconductor Layers for TFT Application

Annex D – Continued.

B3	Original	80	0.5	30	5		
C1	1 part of original to 3 parts of solvent (1:3)	40	0.5	15	5		
C2	1 part of original to 3 parts of solvent (1:3)	20	0.5	15	5		

Spray Coating of Oxide and Chalcogenide Semiconductor Layers for TFT Application

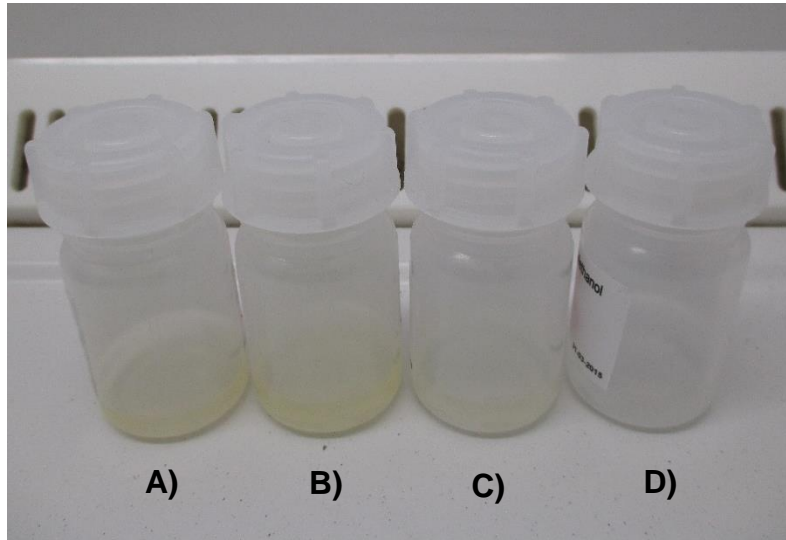
Annex D – Continued.

E1	1 part of original to 3 parts of solvent (1:3)	30	0.1	40	9		
E2	1 part of original to 3 parts of solvent (1:3)	30	0.1	60	9		
E3	1 part of original to 3 parts of solvent (1:3)	30	0.1	120	9		

Spray Coating of Oxide and Chalcogenide Semiconductor Layers for TFT Application

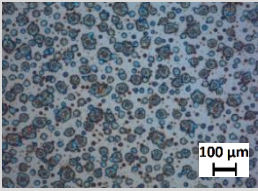
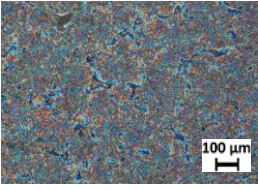
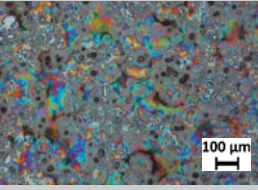
Annex E – Optical images of solutions with different solvents. A – Water; B- Isopropanol and water in a 1:3 proportion; C – Isopropanol and water in a 3:1 proportion; D – Methanol.

It is possible to see that solvents A, B and C do not dissolve the precursor salts (the solution presents a yellow coloration). Only solvent D, methanol produces a clear, transparent solution.



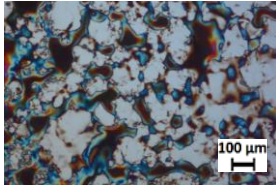
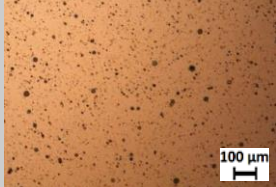
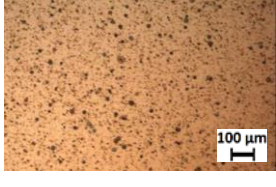
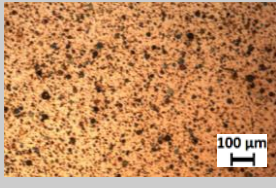
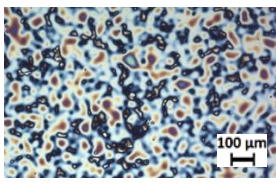
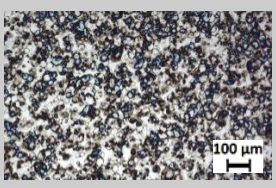
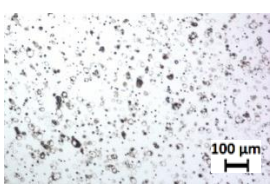
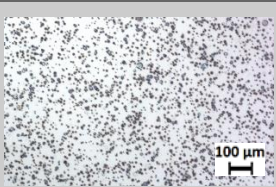
Annex F - Deposition parameters used in spray coating deposition of different samples of SnS thin-films and respective optical images.

T – substrate temperature during deposition; FR – flow-rate of solution; t – deposition time; H – distance between nozzle and substrate.

Sample	Solution	T (°C)	FR (mL/min)	t (s)	H (cm)	Optical Images
F1	0.1 M of SnCl ₂ .2H ₂ O and 0.2M of CH ₄ N ₂ S	250	0.5	30	5	
F2	0.1 M of SnCl ₂ .2H ₂ O and 0.2M of CH ₄ N ₂ S	250	1	30	5	
F3	0.1 M of SnCl ₂ .2H ₂ O and 0.2M of CH ₄ N ₂ S	250	2	30	5	

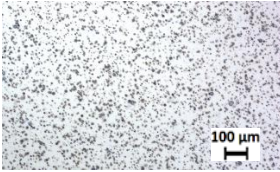
Spray Coating of Oxide and Chalcogenide Semiconductor Layers for TFT Application

Annex F – Continued.

F4	0.1 M of SnCl₂·2H₂O and 0.2M of CH₄N₂S	250	3	30	5	
G1	0.1 M of SnCl ₂ ·2H ₂ O and 0.2M of CH ₄ N ₂ S	350	0.5	30	5	
G2	0.1 M of SnCl ₂ ·2H ₂ O and 0.2M of CH ₄ N ₂ S	350	0.5	60	5	
G3	0.1 M SnCl ₂ ·2H ₂ O and 0.2M CH ₄ N ₂ S	350	0.5	120	5	
H1	0.1 M of SnCl ₂ ·2H ₂ O and 0.2M of CH ₄ N ₂ S	150	0.5	60	5	
H2	0.1 M of SnCl ₂ ·2H ₂ O and 0.2M of CH ₄ N ₂ S	200	0.5	60	5	
H3	0.1 M of SnCl ₂ ·2H ₂ O and 0.2M of CH ₄ N ₂ S	250	0.5	60	5	
H4	0.1 M of SnCl ₂ ·2H ₂ O and 0.2M of CH ₄ N ₂ S	300	0.5	60	5	

Spray Coating of Oxide and Chalcogenide Semiconductor Layers for TFT Application

Annex F – Continued.

H5	0.1 M of SnCl ₂ ·2H ₂ O and 0.2M of CH ₄ N ₂ S	350	0.5	60	5	
-----------	---	-----	-----	----	---	---
